CHAPTER V

Investigation on the Particle Size Reduction of Norfloxacin Hydrates by Thermal Dehydration

5.1 INTRODUCTION

According to the finding that large particles of beclomethasone dipropionate monohydrate (BDM) could turn to small particles of anhydrous beclomethasone dipropionate (BD) via thermal dehydration (Narueporn Nachiengtung, 1997 and Amolwan Chinapak, 2000). This complex phenomenon was studied to evaluate the factors and mechanism that controlled the alteration of particle size of BDM. Other researchers also observed the occurrence of this specific behavior with other organic hydrates. Researchers revealed that different solvation state behaved differently upon desolvation (Perlovich et al., 1996 and 1998). However, the effect of different stoichiometry of hydrates on the particle size reduction via thermal dehydration has not been investigated elsewhere. Norfloxacin (NF), a model organic compound, which was previously studied on the state of hydration and its interconversion was selected. Hence, it was an interesting issue if the dehydration of different NF hydrates would have a particle size reduction effect.

The aim of this study was to evaluate the possibility of particle size reduction via thermal dehydration with respect to different stoichiometry of NF hydrates. In addition, the relationship between either the dehydration energy or the particle size reduction energy versus the stoichiometry of NF hydrates will also be determined.

5.2 EXPERIMENTAL

5.2.1 CHEMICALS

- Norfloxacin dihydrate
- Norfloxacin hemipentahydrate
- Norfloxacin trihydrate
- Norfloxacin pentahydrate
- Isopropyl myristate (supported by Aketrong Chemicals)

5.2.2 INSTRUMENTS

- Differential Scanning Calorimeter (822^e, Mettler Toledo, Switzerland)
- Thermogravimetric Analyzer (TGA/SDTA851^e, Mettler Toledo)
- Hot stage (FP90, Mettler Toledo, Switzerland) equipped with optical microscope (Eclipse E2000, Nikon, Japan)
- Standard sieve analyzer (FT-150M, Filtra vibraciòn, Spain)
    - Sieve mesh No 60 (equivalent to 250 micron)
    - Sieve mesh No 100 (equivalent to 150 micron)
- X-ray Powder Diffractometer (D5000, Siemens, Germany)
- Scanning Electron Microscope (JSM-5410 LV, Jeol, Japan)
- Laser diffraction particle size analyzer (Mastersizer S, Malvern, UK)

5.2.3 METHOD

Preparation of NF Hydrates

Dihydrate NF, hemipentahydrate NF, trihydrate NF and pentahydrate NF were prepared from the anhydrous NF Form A as in chapter IV. They were characterized by differential scanning calorimetry (DSC), thermogravimetry (TGA) and X-ray powder diffractometry (XRPD).

Isothermal Dehydration of NF Hydrates

In order to control the effect of particle size on thermal dehydration, particle sizing was carried out with sieve analysis. The particle sizes of sample were in the range of 150 to 250 microns by using sieve No. 100 and No. 60, respectively.

Isothermal dehydration of NF hydrates was performed by isothermal DSC (IDSC). Four levels of isothermal dehydration temperatures (T_{iso}) were 80 °C, 85 °C, 90 °C and 95 °C. Each sample was weighed approximately 20 mg and placed in aluminum pan (100 μl) with manually pierced lid and sealed. It was then positioned onto DSC and the power level of DSC was monitored as a function of dehydration time (t_{iso}). Nitrogen gas, with a flow rate of 60 ml/min, was purged into the system as a protective gas to prevent any possible oxidative reaction at high temperature.

From the preliminary test, the t_{iso} for different NF hydrates were varied depending on the nature of the hydrate structures. The results showed that trihydrate NF and pentahydrate NF consisted of two steps of dehydration. Thus, the solid samples for the above NF hydrates were investigated at the end of each dehydration step. Unfortunately, hemipentahydrate NF did not show distinct steps of dehydration like trihydrate NF and pentahydrate NF. Therefore, the solid sample of hemipentahydrate was only obtained at the end of complete dehydration test.

The water content, particle size and crystal structure of dehydrated NF hydrates were measured by TGA, laser diffraction particle size analyzer and XRPD, respectively. The physical appearance of dehydrated sample was also observed with scanning electron microscope (SEM).

Characterization of NF Hydrates

Thermal Analysis

The thermal properties of NF hydrates were evaluated by DSC in conjunction with STAR^e software. The sample weight of approximately 5 to 10 mg was placed in standard aluminum pan (40 µl) and sealed with pierced lid. The scanning rate was 10 °C/min and the temperature range was 30 to 230 °C. Dried nitrogen gas at the rate of 60 ml/min was purged all throughout the study to avoid oxidative decomposition upon heating.

Weight loss of NF hydrates produced were analyzed using TGA. The sample container, heating condition were the same as that utilized in DSC study. The experiment was done in triplicate. Net change in mass was determined to disclose the stoichiometry of crystalline water.

X-ray Powder Diffraction (XRPD)

XRPD using CuKα generator at 40kV and 20mA was used to determine the characters of NF hydrates produced and the solid obtained after dehydration. The scan speed, scan step and angular scan range was set at 5° per min, 0.04° per step and 5 to 35° 2θ, respectively.

Particle Size Analysis

Laser diffraction particle size analyzer with wet method was employed. A dispersion medium of isopropyl myristate (IPM) was selected in order to prevent the transformation of NF hydrates to a more stable pentahydrate NF during the determination. In addition, mild agitation was done during the observation to minimize aggregation of the sample after being dispersed. The particle size measurement was done in triplicate.

Scanning Electron Microscope (SEM)

The morphology of the NF hydrates both before and after dehydration were investigated by SEM. The sample powder was carefully placed on the metal stub. It was then coated with gold before its morphology was recorded.

Determination of Dehydration Energy of NF Hydrates

Quantitative determination of energy used during dehydration was calculated based on the concept of the area under the curve (AUC) of IDSC thermogram. Total AUC obtained by trapezoidal rule from energy consumption-dehydration time profile was defined as the dehydration energy (Kishore, 1978). In addition, the determination of AUC of the dehydration of NF hydrate was specifically defined due to an uncommon IDSC thermogram seen from preliminary studies (Figure 5.1). During the early period of experiment, the power of IDSC was increase due to the equilibration of system (from point A to B). The later step from point B to C was an endothermic dehydration reaction. Thus, the extrapolation from point B to A' was additionally done and calculated as a part of the total AUC. Therefore, the total AUC was equivalent to the summation of the AUC of early stage of dehydration (from A' to B) and the AUC of the later stage of dehydration (from B to C).

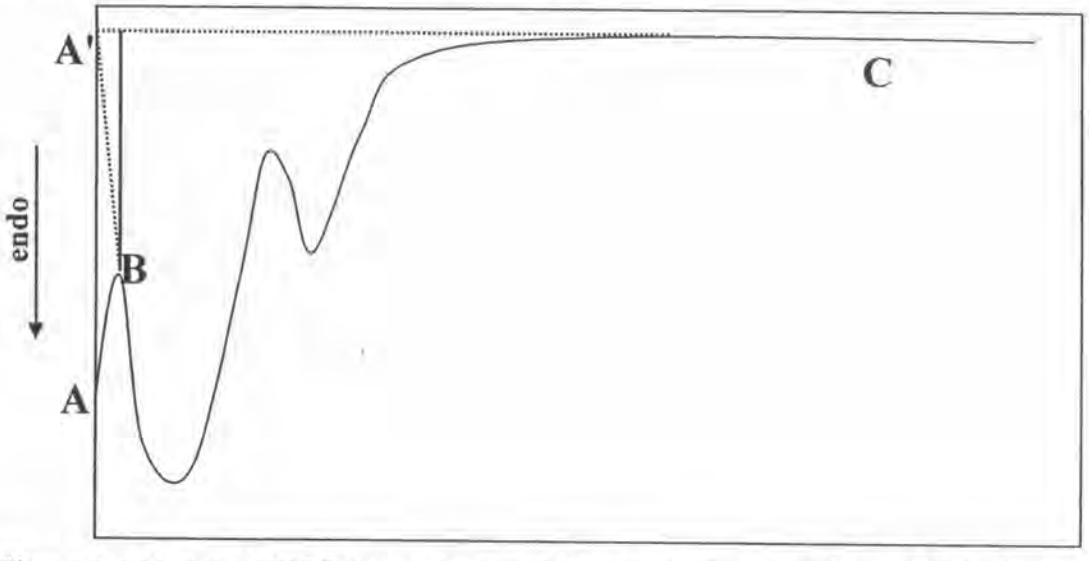

Figure 5.1 Model of IDSC thermogram of NF hydrate during isothermal dehydration

On the other hand, the calculation of activation energy (E_a) for dehydration was determined by both model dependent and model independent solid state kinetic. Model dependent kinetic was determined from a plot of ln k from the solid state kinetic model versus reciprocal absolute temperature (1/T) provides E_a of dehydration from the slope ($-E_a/R$) (Byrn et al., 1999). Model independent kinetic, the slope from linear relationship of ln t and 1/T was calculated and resolved as E_a of dehydration (Dong et al., 2002 and Zhou et al., 2003).

5.3 RESULTS AND DISCUSSION

Isothermal Dehydration of Dihydrate NF

Due to a difficulty in the reproducible production of dihydrate NF, the amount of dihydrate NF was very limited. Therefore, this study could not be performed with a typical IDSC as described in the experimental method section due to limited amount of sample. Thermo microscopy was alternatively chosen as preliminary investigation on the particle size reduction via thermal dehydration. Single particle of dihydrate NF was placed on glass slide over heating station of hot stage (HSM) without immersing oil under different T_{iso}. The t_{iso} was applied of up to 6 hours.

HSM results revealed that dihydrate NF lost an anisotropic property with respect to heating time at every T_{iso}. Disappearance of anisotropy was seen from the development of opaque region from outer part towards the inner core of the crystal (Figure 5.2). The unilluminated phase of dihydrate NF was found to be due to a dehydration process during molecular rearrangement in the crystal lattice (Byrn et al., 1999). Thus, the dehydration time was directly proportional to the time used to obtain total unilluminated phase. The results showed the time for total unilluminated phase at 80 °C and 85 °C were approximately 10 mins and at 90 °C and 95 °C were approximately 5 mins. The higher T_{iso} resulted in shorter dehydration time. The small particle of dehydrated dihydrate NF was not generated at every T_{iso} used. However, SEM of all heated dihydrate NF only showed cracks around external surface of the crystal (Figure 5.3). Thermal dehydration could not destroy dihydrate NF particle, the structural arrangement was stable even after all the water molecules were removed and could not damage the dihydrate NF to a small particle of anhydrous NF.

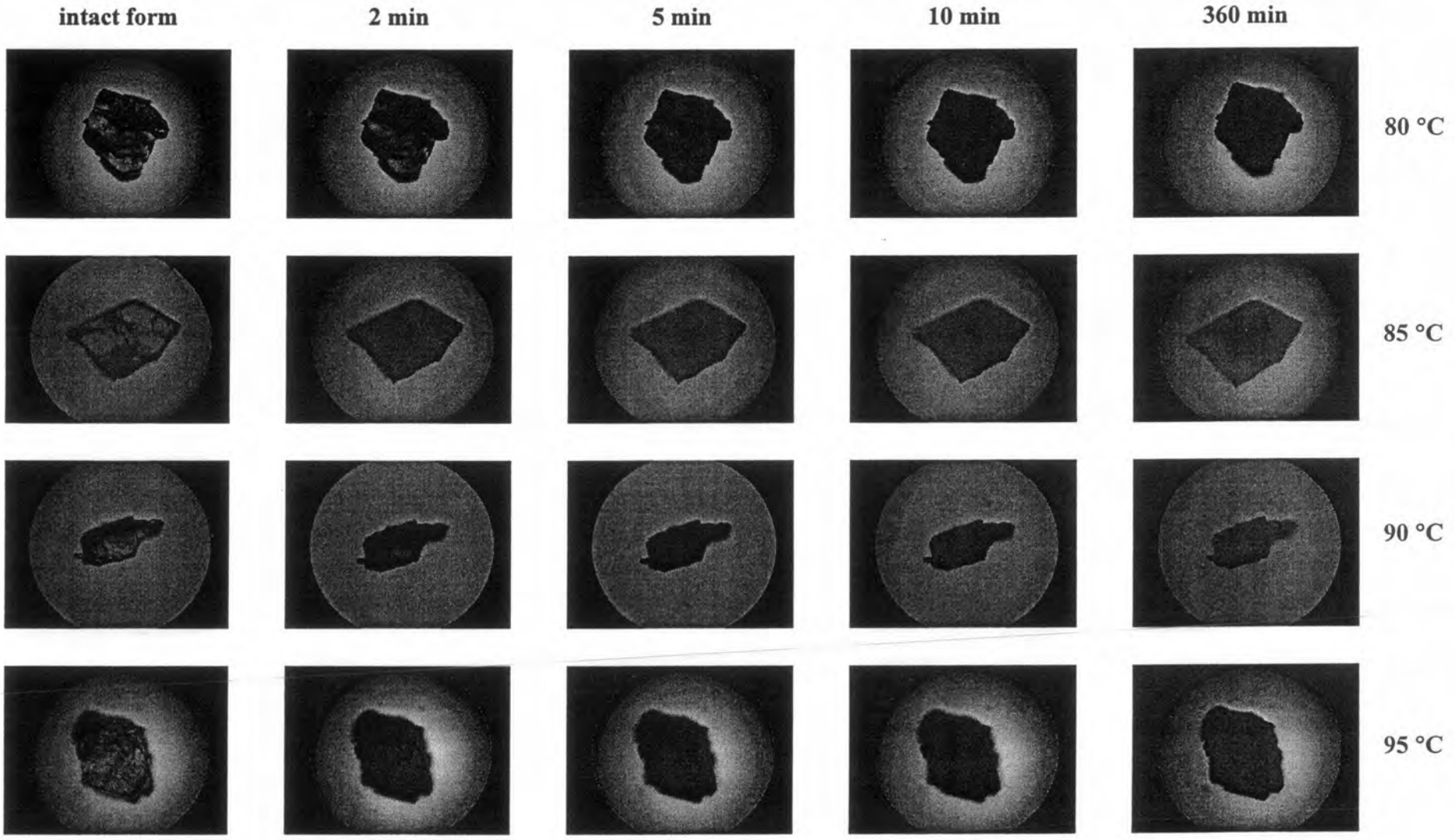

Figure 5.2 Photomicrographs of dihydrate NF during isothermal dehydration at various T_{iso} as a function of heating time

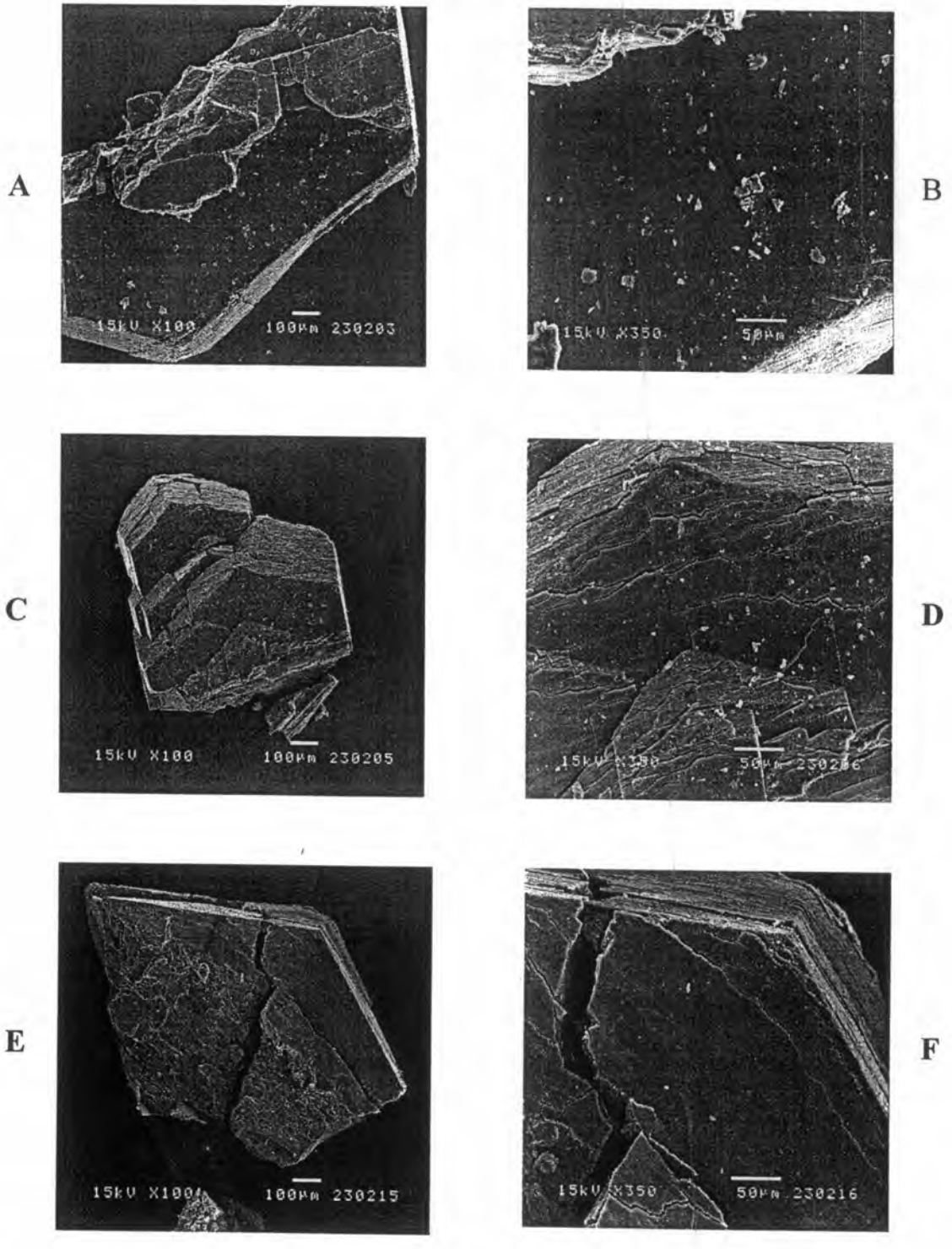

Figure 5.3 SEM photomicrographs of dihydrate NF after 360 mins of isothermal dehydration with respect to different T_{iso}. (A and B – intact dihydrate NF, C and D – 80 °C of isothermal dehydration, E and F - 85°C of isothermal dehydration)

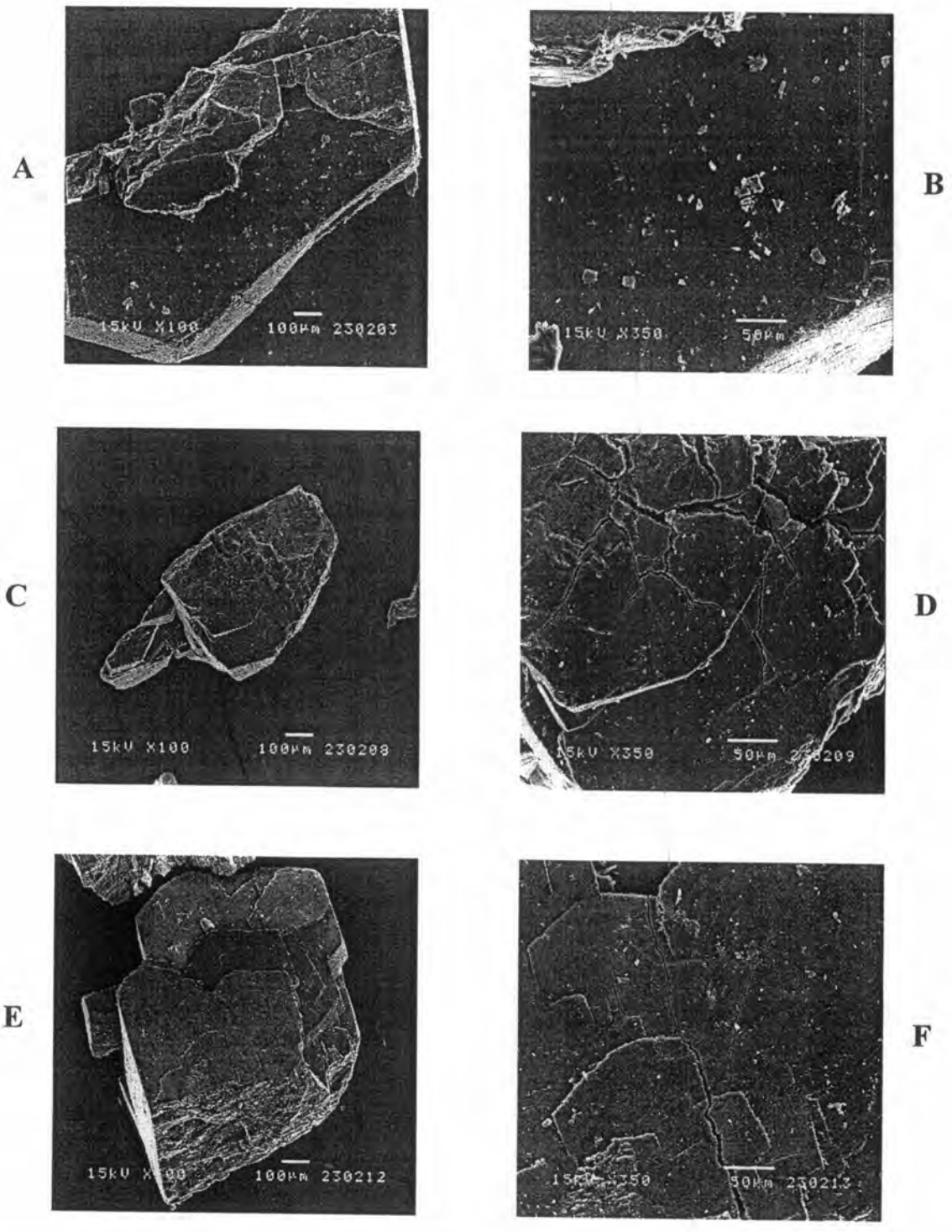

Figure 5.3 (cont.) SEM photomicrographs of dihydrate NF after 360 mins of isothermal dehydration with respect to different T_{iso}. (A and B – intact dihydrate NF, C and D – 90 °C of isothermal dehydration, E and F - 95°C of isothermal dehydration)

Explanation of unchanged particle size of dihydrate NF during thermal dehydration of two molecules of crystalline waters was of great interest. The single crystal structure of dihydrate NF has already been resolved (Chapter IV). Hydrogen bond acted as dominant bonding for NF amidst water in the crystal lattice. An atomic position of NF and waters in the dihydrate structure is shown in Figure 5.4. There were five hydrogen bonds in dihydrate NF that played a major role to stabilize the crystalline water in the dihydrate structure (Figure 5.5). The hydrogen bonds in dihydrate NF structure were moderate hydrogen bonding. Two hydrogen bonds were moderate to strong bonding while the other three bonds were moderate to weak bonding (Table 5.1). The primary water molecule (O1) connected to two NF moieties with two moderate to weak hydrogen bonds and also bound to the secondary water (O2) with a moderate to weak hydrogen bond. The secondary water molecule (O2) directly connected to two molecules of NF with moderate to strong hydrogen bonds and acted as a main barrier on dehydration. It showed that the second water of crystallization molecule was bound to NF moiety stronger than the primary water. In addition, DSC thermogram of dihydrate NF obtained in chapter IV was shown to have two consecutive endotherms. It was assumed that the primary water molecule was theoretically removed from the dihydrate structure before the secondary water molecule. However, these two events for liberating the water molecules could not be distinctly separated. The water tunnel in dihydrate NF structure was also observed. It showed only one open-end tunnel along the *c* axis that allowed the easy removal of water molecule (Figure 5.6).

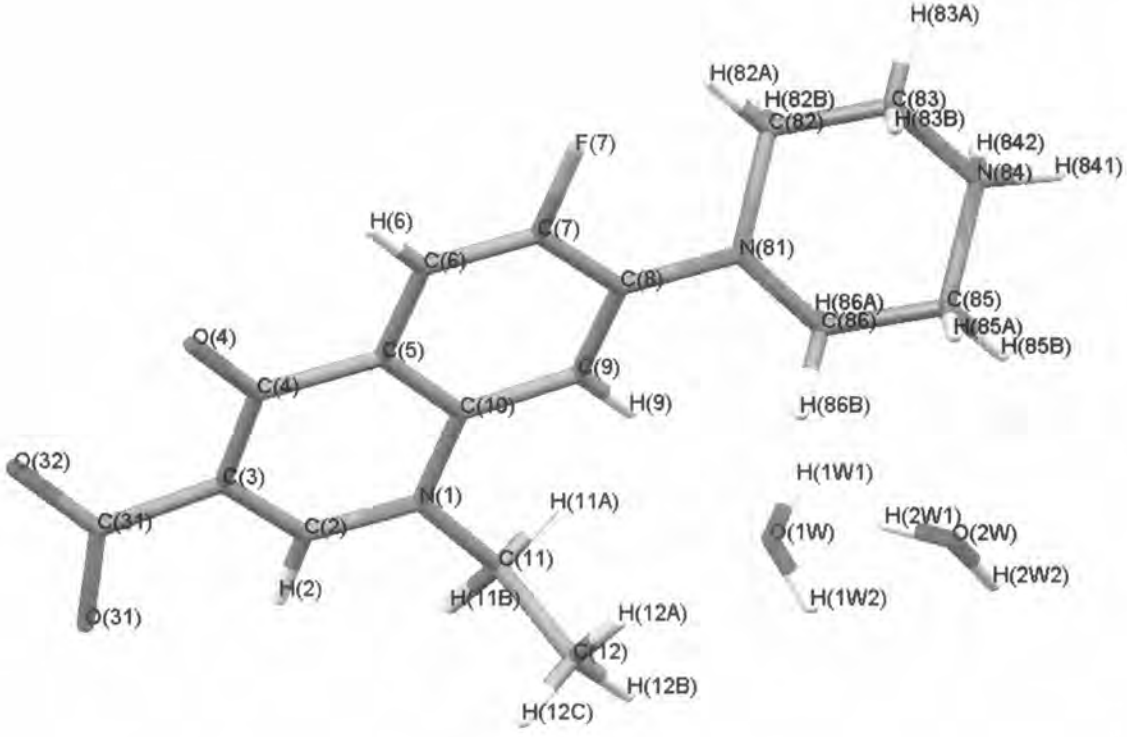

Figure 5.4 The atomic positions of NF moiety and water of crystallization molecules of dihydrate NF

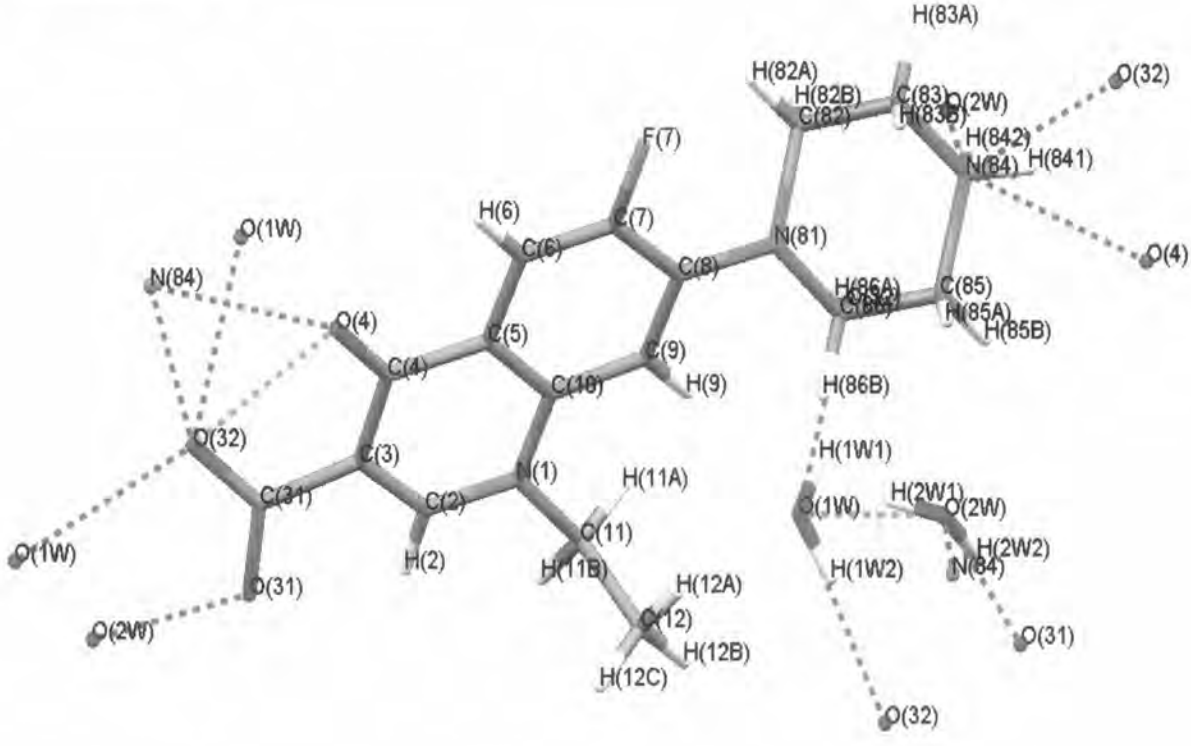

Figure 5.5 The hydrogen bonding in crystal lattice of dihydrate NF structure

Table 5.1 The hydrogen bond positions and molecular property in dihydrate NF crystal structure from crystallographic data

Bond definition	Hydrogen bond position	Bond length (Å)	Bond angle(°)	Type of hydrogen bond
	O(1W)-H(1W2)-O(32)			
A----B	O(1W)-O(32)	2.865	172.58	Moderate to
H-A	O(1W)-H(1W2)	0.896		weak
H----B	H(1W2)-O(32)	1.974		
	O(1W)-H(1W1)-O(32)			
A----B	O(1W)-O(32)	2.986	163.24	Moderate to
H-A	O(1W)-H(1W1)	0.950		Weak
H----B	H(1W1)-O(32)	2.064		
	O(1W)-H(2W1)-O(2W)			
A----B	O(1W)-O(2W)	2.783	153.81	Moderate to
H-A	O(1W)-H(2W1)	0.880		weak
H----B	H(2W1)-O(2W)	1.966		
	O(2W)-H(2W2)-O(31)			
A----B	O(2W)-O(31)	2.625	169.81	Moderate to
H-A	O(2W)-H(2W2)	0.967		strong
H----B	H(2W2)-O(31)	1.668		
	O(2W)-H(842)-N(84)			
A----B	O(2W)-O(2W)	2.712	169.26	Moderate to
H-A	O(2W)-H(842)	1.040		strong
H----B	H(842)-N(84)	1.684		

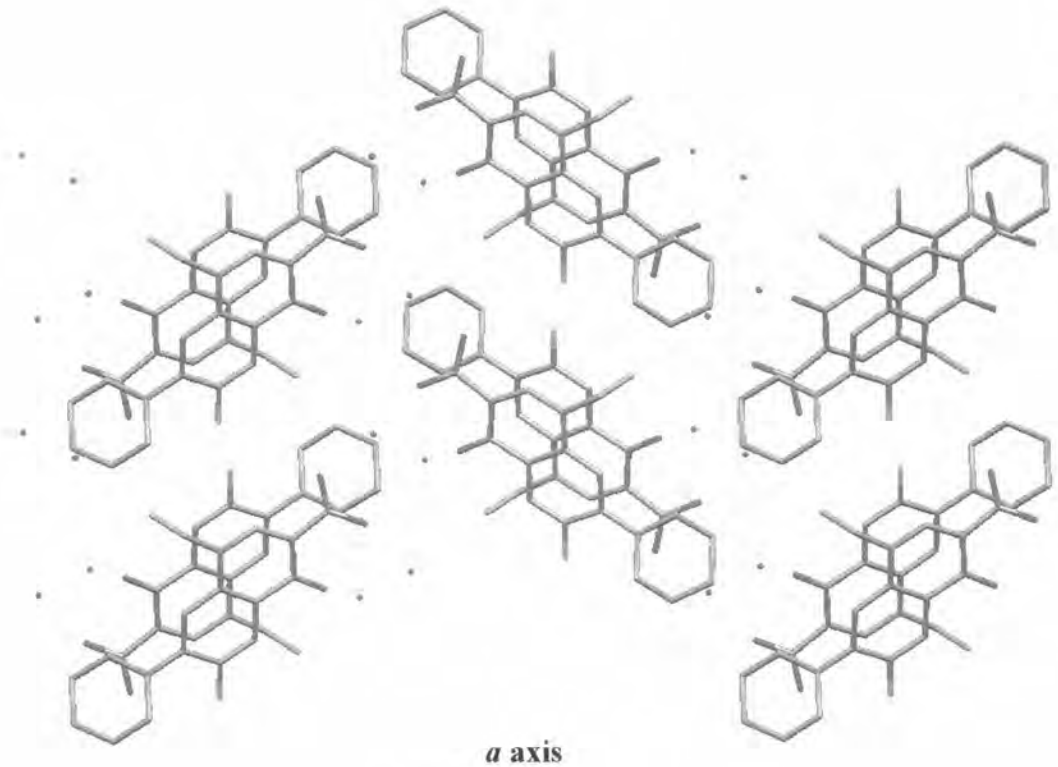

***a* axis**

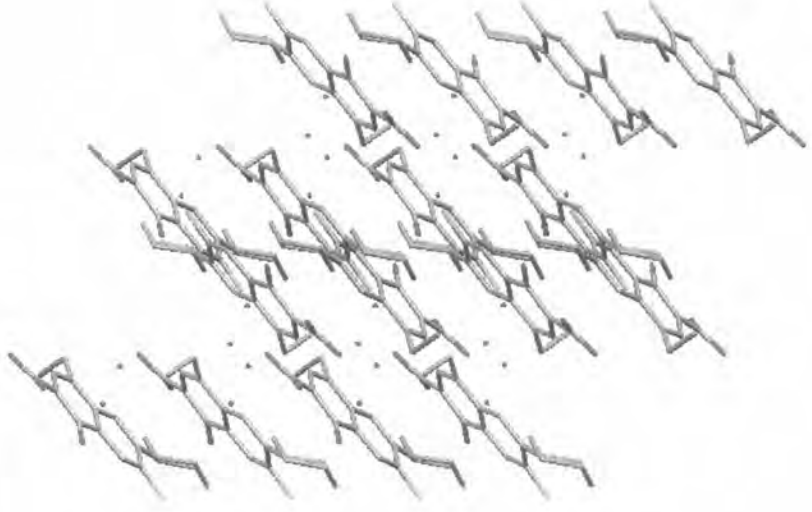

***b* axis**

Figure 5.6 The crystallographic arrangement of water channel in dihydrate NF structure along different unit cell axis (free red dots are crystalline water).

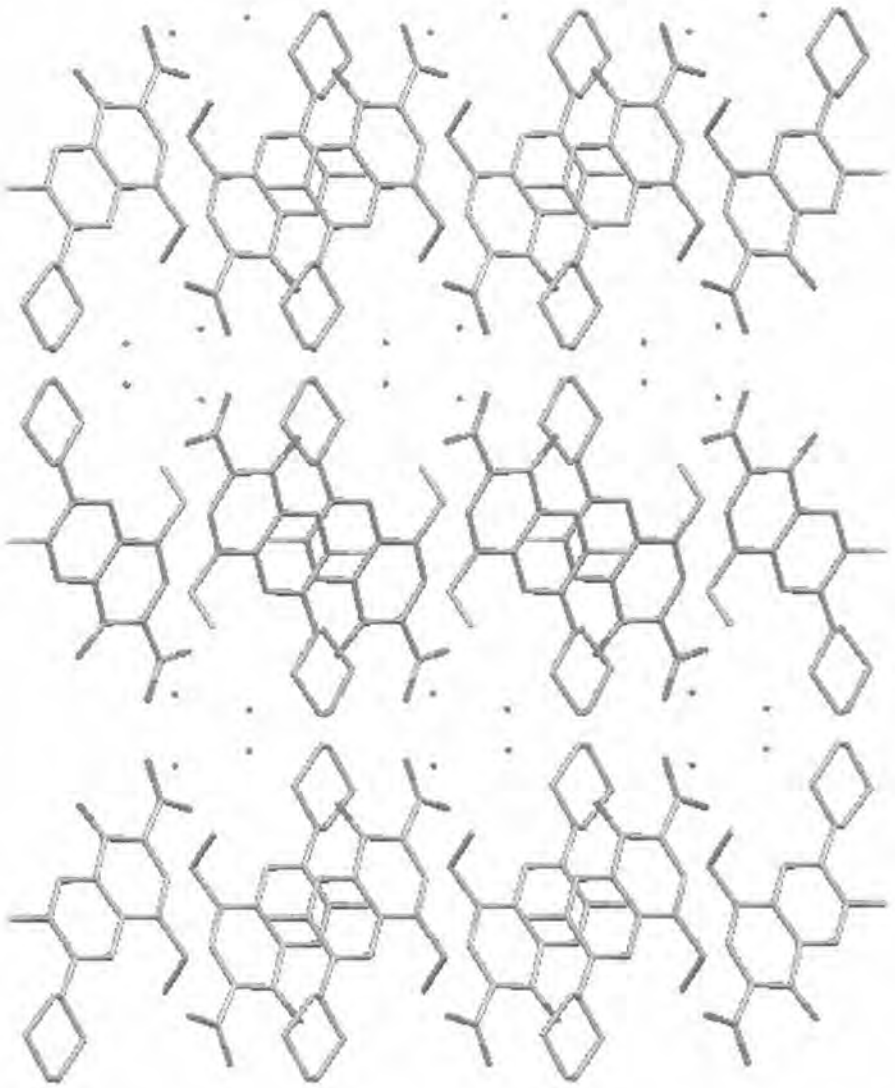

***c* axis**

Figure 5.6 (cont.) The crystallographic arrangement of water channel in dihydrate NF structure along different unit cell axis (free red dots are crystalline water)

In addition, the concept of the compactness of solvent packing or K_{chan} was also considered (Perlovich et al., 1996 and 1998). As mentioned in Chapter IV, the more compact the crystal packing the higher the K_{chan} value and resulted in the difficulty of dehydration. The crystallographic data of NF dihydrate were reported by Florence et al. (2000) and was generated from our experiment in Chapter IV. Z value and unit cell volume of NF dihydrate structure are 4 and 1604.8 $Å^3$, respectively (Table 5.2). On the other hand, the essential data for the calculation of K_{chan} was a unit cell volume of the anhydrous NF Form A which was never reported elsewhere. There were two methods to obtain this data. The first method, a perfect crystal of anhydrous

NF must be generated and resolved by single crystal X-ray diffractometry. Several attempts to generate suitable crystal of anhydrous NF Form A were performed in this experiment but it was not successful. An alternative method was to employ the XRPD data. Software for crystal structure elucidation "PowderSolve®" under the license of Material Studio®, was used to elucidate the best possible anhydrous NF Form A crystal structure.

Table 5.2 Crystal data of dihydrate NF

Crystal data	Dihydrate NF
Empirical formula	$C_{16}H_{18}FN_3O_3.2H_2O$
Molecular weight	355.34
Space group	Monoclinic
	$P2_1/C$
a (Å)	8.2835
b (Å)	21.7276
c (Å)	9.5436
β	110.886
crystal cell volume ($Å^3$)	1604.8
Z	4

The first step of elucidation was the indexing of the unit cell with "Powder Indexing Program" by high quality XRPD pattern as an input data (Appendix D) and refined the simulated unit cell by "Powder Refinement Program". Finally, the PowderSolve program was employed at the final stage of crystal structure elucidation. In this experiment, Powder Indexing and Powder Refinement programs generated different possible unit cells with different space group as seen in Table 5.3. However, these data could not be finalized by PowderSolve program to generate only one accurate crystal structure of anhydrous NF Form A. Although the single correct crystal structure of anhydrous NF Form A was not obtained, the unit cell volume from Powder Indexing program could be used to roughly determine the K_{chan} of dihydrate NF. Powder Indexing program generated the several space groups with different unit cell volumes, the higher figure of merit (FOM) of the result from indexing generally indicated the more accurate unit cell data. From Table 5.3, the monoclinic space

group with unit cell volume of 3682.59 $Å^3$ had a highest FOM. However, it was larger than the unit cell volume of dihydrate NF (1604.8 $Å^3$). In general, the unit cell volume of the anhydrous structure should be lower than the unit cell volume of the hydrated structure. Thus, the monoclinic space group with highest FOM was not used for the determination of K_{chan}. The other results obtained by indexing, the four triclinic structures, showed high FOM with lower unit cell volume when compared to the unit cell volume of the dihydrate NF. These unit cell volume values were employed as representatives for possible anhydrous NF Form A unit cell volume.

The K_{chan} of dihydrate NF were calculated based on the unit cell volume of anhydrous NF Form A with the triclinic space group and are presented in Table 5.3. The estimated K_{chan} of dihydrate NF were in the range of 0.3368-0.6780. It was higher than those of risedronate sodium hemipentahydrate (equal to 0.1370) (Lester et al., 2006) and BDM (equal to 0.1663) (Chapter III). These results indicated that water of crystallization in dihydrate NF structure occupied the void space of around 33% to 68%. There was less free volume to allow for water mobility. Furthermore, a more close packing induced a strong hydrogen bonding between water and active species and led to higher bonding energy. Therefore, high value of K_{chan} in dihydrate NF supported the stability of crystal lattice during dehydration. In conclusion the main reason for dihydrate NF to retain the crystal size after dehydration largely depends on

1. The structure of dehydrated NF composed of moderate to strong hydrogen bonds
2. There was only one direction of water tunnel
3. The high compactness of solvent packing (K_{chan}).

Thus, the opportunity for the structure to collapse after dehydration and eventually led to significantly smaller particles of dihydrate NF was unlikely and the apparent particle size reduction energy was impossible to calculate. Therefore, the future experimental sections will only focused on the dehydration behavior and the energy involved in the process.

Table 5.3 Crystallographic data of anhydrous NF Form A obtained from Powder Indexing program of MATERIAL STUDIO® software simulated with XRPD data

	Figure of Merit (FOM)	K_{chan} of dihydrate NF	Peak Used*	Unit cell							
				system	a (Å)	b (Å)	c (Å)	α (°)	β (°)	γ (°)	Volume ($Å^3$)
1	2.20	-	22 of 22	Monoclinic	21.13912	15.69688	13.03046	90	121.60200	90	3682.59
2	2.00	0.3368	22 of 22	Triclinic	18.75665	12.96237	7.23957	126.21100	92.06500	101.24500	1367.25
3	2.10	0.5878	23 of 23	Triclinic	20.72207	12.81180	7.80562	125.57900	114.38100	88.58800	1468.71
4	1.90	0.3834	22 of 22	Triclinic	20.08745	12.87875	7.25269	55.86900	107.98300	115.49700	1396.15
5	1.70	0.6780	23 of 23	Triclinic	18.42371	10.54013	8.02520	75.16900	93.56300	99.18300	1486.81
6	1.50	-	22 of 22	Monoclinic	31.18705	4.15313	29.05046	90	106.36700	90	3610.24

* The list of peaks used for indexing (Appendix D)

Isothermal Dehydration of Hemipentahydrate NF

IDSC patterns during dehydration of hemipentahydrate NF are illustrated in Figure 5.7. The t_{iso} of hemipentahydrate NF at various T_{iso} were different and depend on the nature of dehydration. The t_{iso} was determined by observing an unchanged power in IDSC thermograms. The t_{iso} of the dehydration of hemipentahydrate NF was determined to be at 180 mins at 95 °C and 300 mins at 80 °C, 85 °C and 90 °C. IDSC patterns of all hemipentahydrate NF showed two steps consecutive dehydration. However, the dehydration steps were not clearly separated. Energy calculation of the dehydration process was possible only when dehydration was completed. The AUC of IDSC patterns at various T_{iso} were calculated and are tabulated in Table 5.4. The result revealed that dehydration energies at every T_{iso} were insignificantly different. It could be concluded that the total energy needed for dehydration of hemipentahydrate NF was temperature independent within the investigated range of 80 °C to 95 °C.

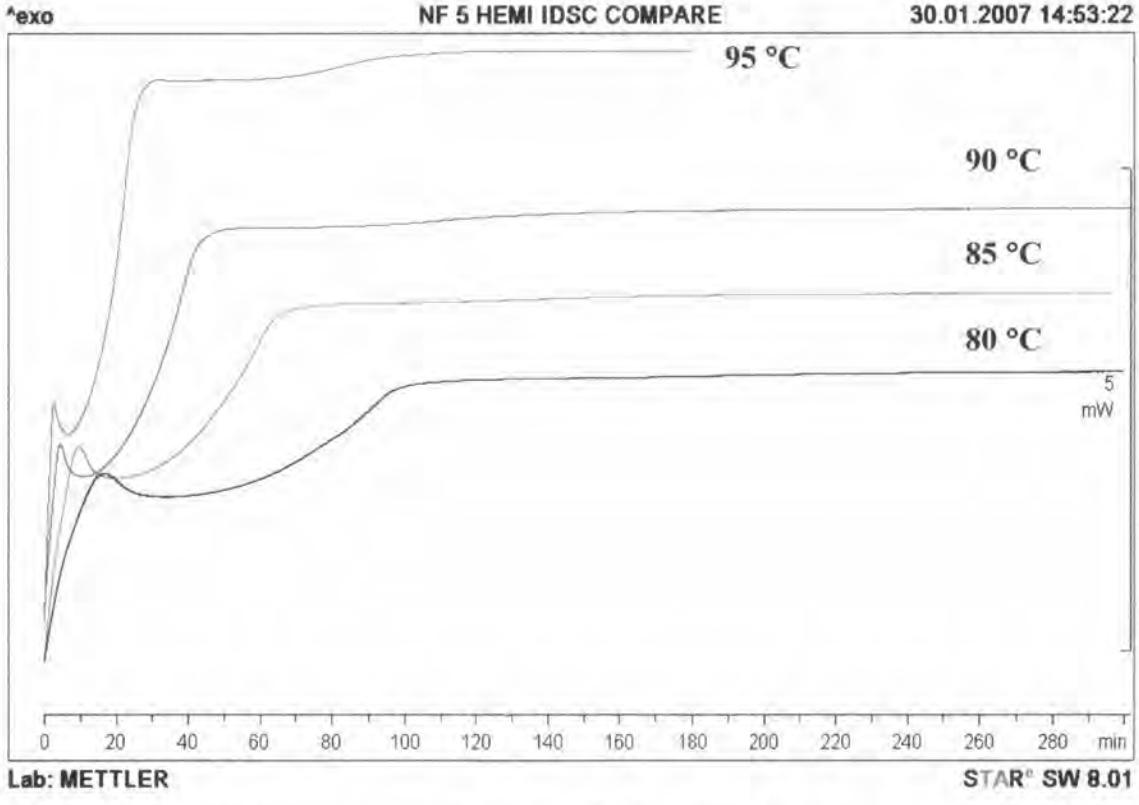

Figure 5.7 IDSC thermograms of hemipentahydrate NF during isothermal dehydration at various T_{iso}

Table 5.4 Dehydration energy, residual water content and particle size of dehydrated hemipentahydrate NF after complete dehydration at different T_{iso}

T_{iso} (°C)	Dehydration energy (J/g)	Residual water content by TGA (%w/w)	d [v,0.5] (micron)
Intact form	-	12.12 ± 0.04	248.88 ± 2.91
80	285.12 ± 5.34	0.38 ± 0.06	240.68 ± 5.53
85	290.33 ± 6.57	0.43 ± 0.36	225.03 ± 8.16
90	292.38 ± 5.75	0.37 ± 0.27	212.17 ± 5.89
95	277.57 ± 12.56	0.24 ± 0.13	237.13 ± 1.50

The residual water contents of all dehydrated hemipentahydrate NF were lower than 1% w/w (Table 5.4) indicating the generation of the anhydrous phase of NF. XRPD of every dehydrated hemipentahydrate NF after exposure to different T_{iso} showed the specific character of anhydrous NF Form A (Figure 5.8).

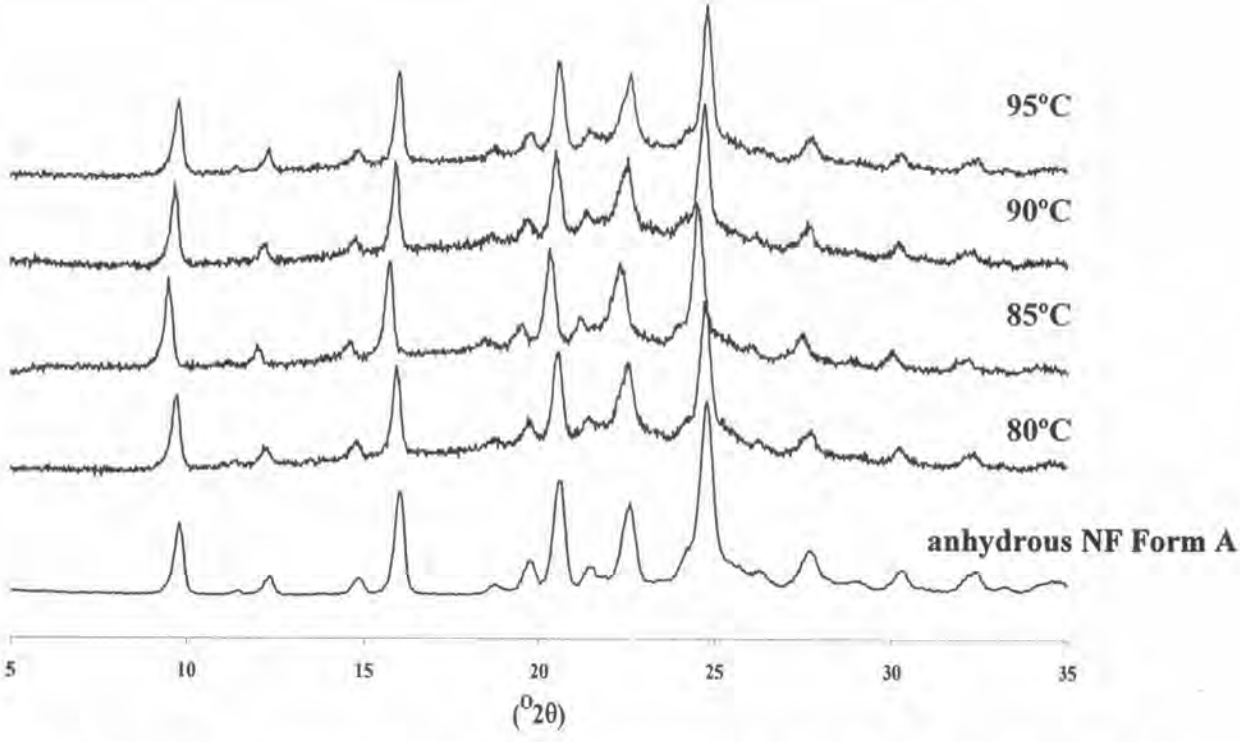

Figure 5.8 XRPD diffractograms of dehydrated hemipentahydrate NF after isothermal dehydration with respect to T_{iso}

Investigation of particle size changes during dehydration are also demonstrated in Table 5.4. According to statistical comparison, the difference of particle size between intact hemipentahydrate NF and all dehydrated hemipentahydrate NF were found to be significantly different ($p<0.05$). The particle sizes of intact hemipentahydrate NF and dehydrated samples at 85 °C and 90 °C were significantly different ($p<0.05$), while there was no difference between the particle size of intact hemipentahydrate NF and the dehydrated samples at 80 °C and 95 °C. This finding was similar to the dehydration of beclomethasone dipropionate monohydrate. It might be due to the fact that the particle size reduction of hemipentahydrate NF depends on the heating rate at different T_{iso} while dehydration energies of all dehydrated samples were similar. At the lowest T_{iso} of 80 °C, SEM photomicrographs did not show particle size disruption (Figure 5.10). SEM photomicrographs of dehydrated hemipentahydrate NF at higher T_{iso} of 85 °C and 90 °C showed surface defects and resulted in the smaller particles of anhydrous NF Form A. However, at the highest T_{iso} of 95 °C, anhydrous barrier was rapidly generated and retard the escape of water molecules and led to the retained hydrated structure. The statistically significant difference in particle size between intact and dehydrated hemipentahydrate NF was determined but it could not be concluded that the particle size reduction was evident such as that of BDM because the maximum difference was within the range of 25 micron. Thus, the apparent energy used for particle size reduction of hemipentahydrate NF by isothermal dehydration was not determined in this study.

The relationship between fraction reacted (α) and time (t) of dehydration of hemipentahydrate NF by model dependent solid state kinetic are presented in Figure 5.9. It was directly derived from IDSC data at each T_{iso} and showed two steps of dehydration from observable two phases of the slopes. The calculated E_a with different solid state kinetic equations were in the range of approximately 76 kJ/mol and 120 kJ/mol for the early and the later stage of dehydration, respectively. The Avrami Erofeev equations with one and two dimensional gave a good fit of the dehydration of hemipentahydrate NF. The random nuclei generated along one or two dimensions and progressively ingested other nuclei was defined as main mechanism of dehydration. Beside, the phase boundaries model also showed good agreement. It indicated the advancement of dehydrated phase from

the outside of particle concerned to the inside. Therefore, the main mechanism of dehydration was not able to be explained by either single Avrami Eroféev model or Phase Boundaries model. Model independent approach resulted in E_a in between of 80 to 120 kJ/mol which was similar to the E_a obtained from model dependent (Figure 5.11). These results indicated that the "rate" of dehydration of hemipentahydrate NF for both steps depended on the dehydration temperature. The higher E_a of the initial step of dehydration strongly indicated the temperature dependency of the dehydration rate. On the other hand, the gradual and continuous decrease in E_a during dehydration indicated less energy barrier for dehydration which resulted from the disruption of the structural integrity of hydrate particles without particle size reduction.

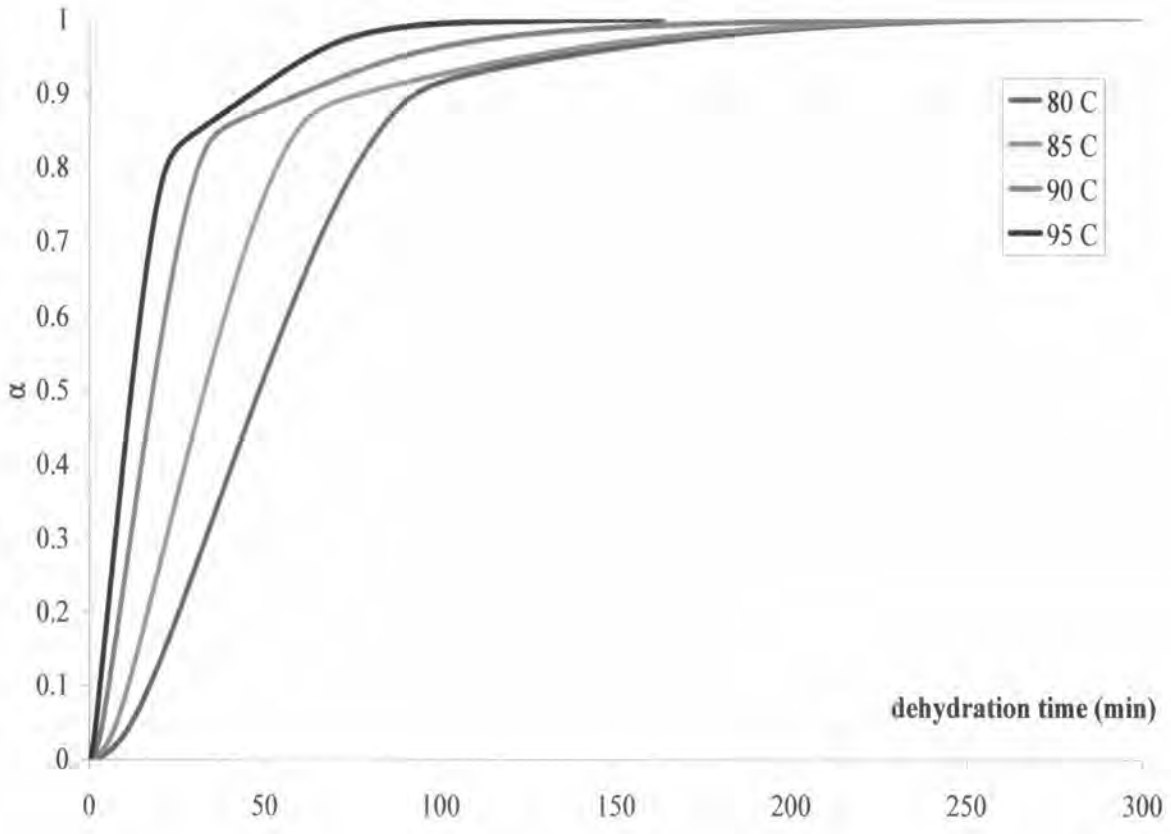

Figure 5.9 α-t curves of dehydration of hemipentahydrate NF at different T_{iso}

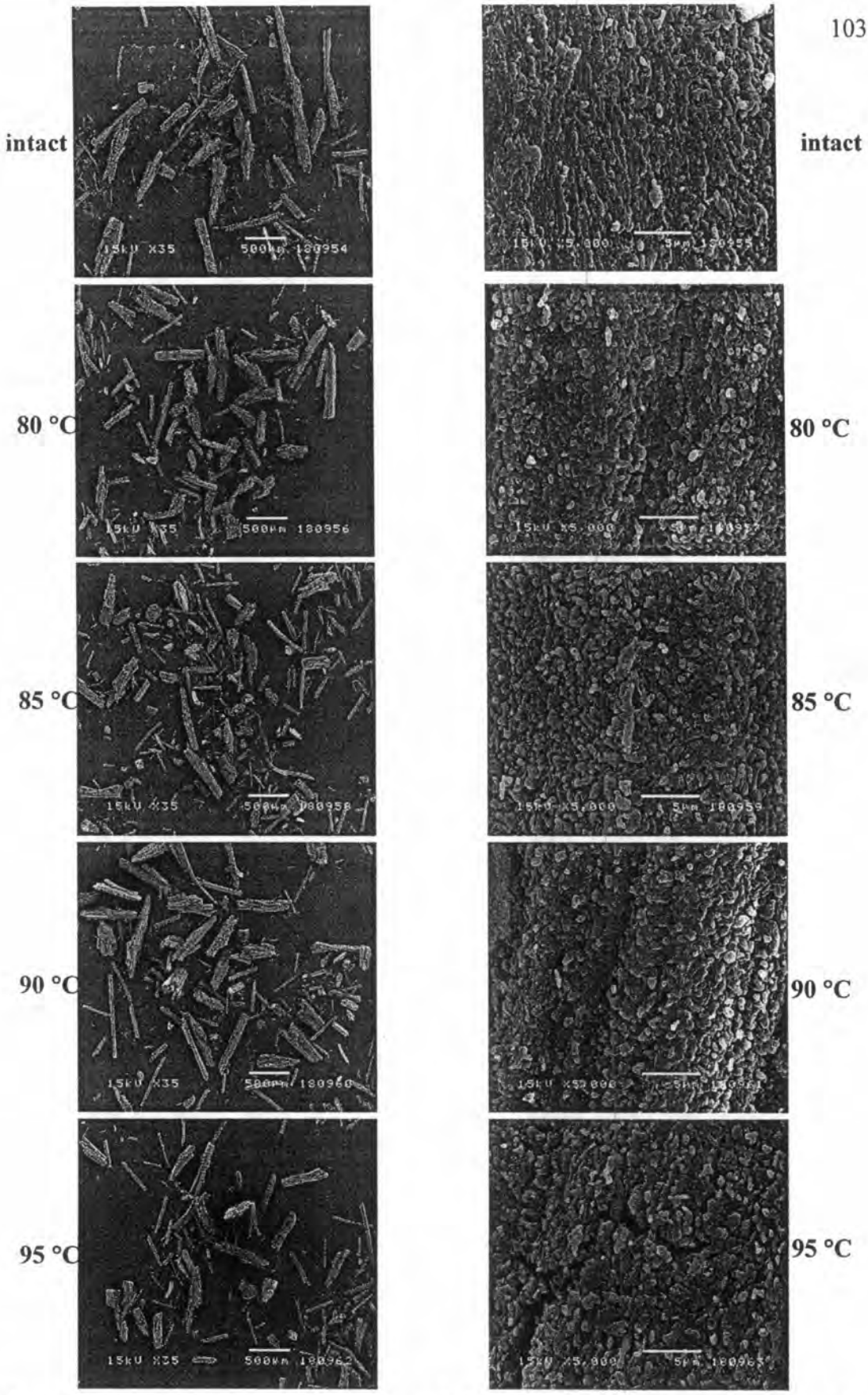

Figure 5.10 SEM photomicrographs of hemipentahydrate NF after complete dehydration at various T_{iso} (left column at the magnification of 35, right column at the magnification of 5000)

Table 5.5 The activation energy of isothermal dehydration of hemipentahydrate NF with various solid state kinetic models

Model equation	E_a (kJ/mol)	
	First step of dehydration (0.20 to 0.80 of α)	Second step of dehydration (0.93 to 0.97 of α)
Avrami Eroféev		
1 dimensional	76.56	119.23
2 dimensional	75.84	119.19
Phase Boundary		
2 dimensional	76.95	120.45
3 dimensional	77.22	121.10

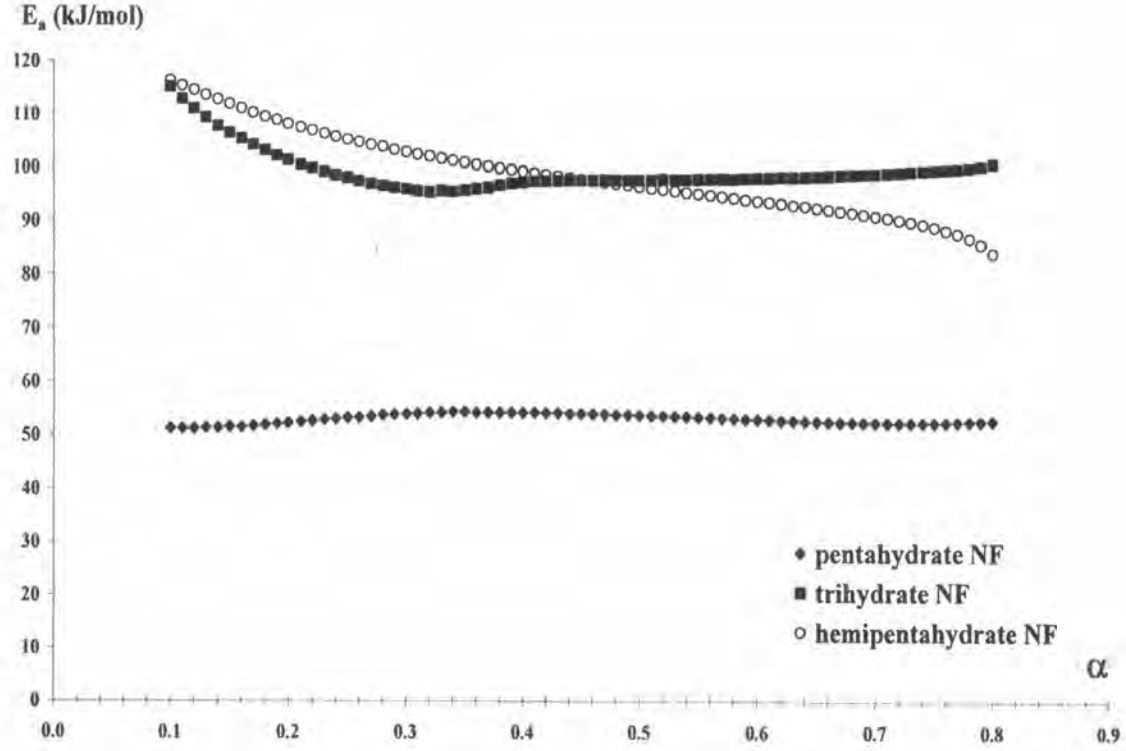

Figure 5.11 Comparative activation energy of dehydration derived from model independent solid state kinetic of different stoichiometric NF hydrates

Isothermal Dehydration of Trihydrate NF and Pentahydrate NF

Due to a complex dehydration behavior of trihydrate NF and pentahydrate NF, IDSC of both hydrate NF (Figure 5.12 and Figure 5.13) showed consecutive dehydration similar to hemipentahydrate NF. However, these behaviors showed clearer separation between two phases of dehydration than that of hemipantahydrate NF. The t_{iso} of trihydrate NF and pentahydrate NF at different T_{iso} were able to be elucidated as two points. The first t_{iso} was selected between the first and second dehydration endotherm while the second t_{iso} was the time of unchanged power of later dehydration phase in IDSC thermogram. In this study, the t_{iso} of first step dehydration for trihydrate NF were 310, 180, 110 and 80 mins while the t_{iso} of second step or complete dehydration were 750, 510, 330 and 210 mins at 80 °C, 85 °C, 90 °C and 95 °C, respectively. On the other hand, the first t_{iso} of pentahydrate NF were 240, 140, 90, 70 mins and the second t_{iso} for complete dehydration were 600, 390, 330, 240 mins at 80 °C, 85 °C, 90 °C and 95 °C, respectively. The direct energy measurement of the first and the second steps (complete dehydration) were determined and tabulated in Tables 5.6 and 5.7. Additional data of residual water content and particle size of each dehydrated sample were also included in these tables.

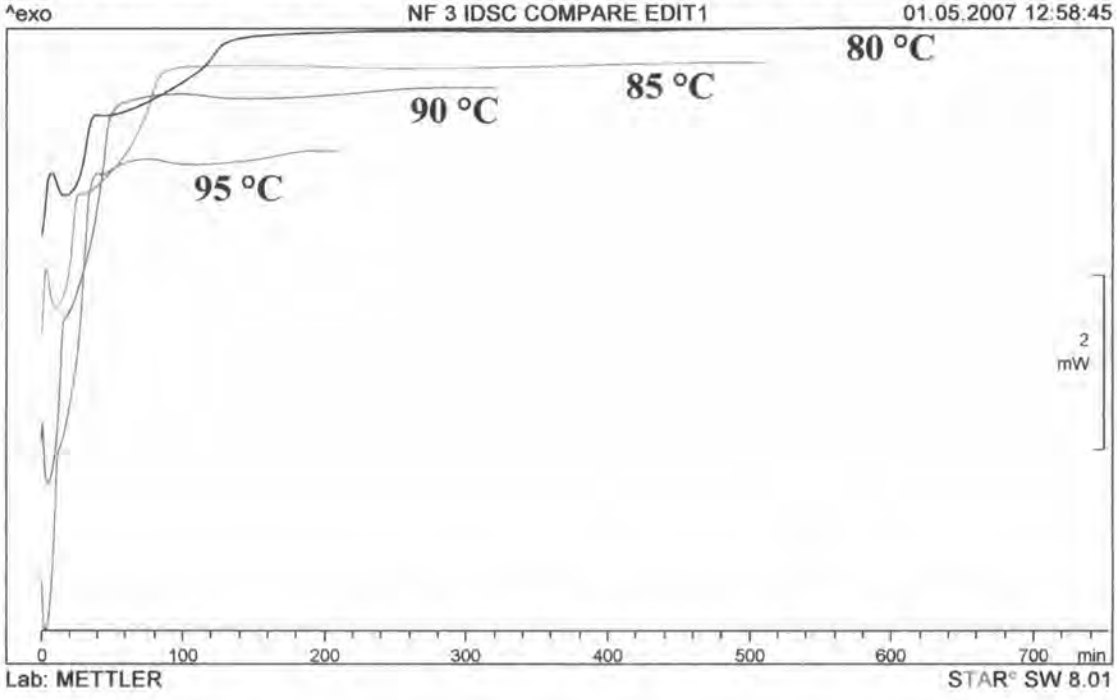

Figure 5.12 IDSC thermograms of trihydrate NF during isothermal dehydration at various T_{iso}

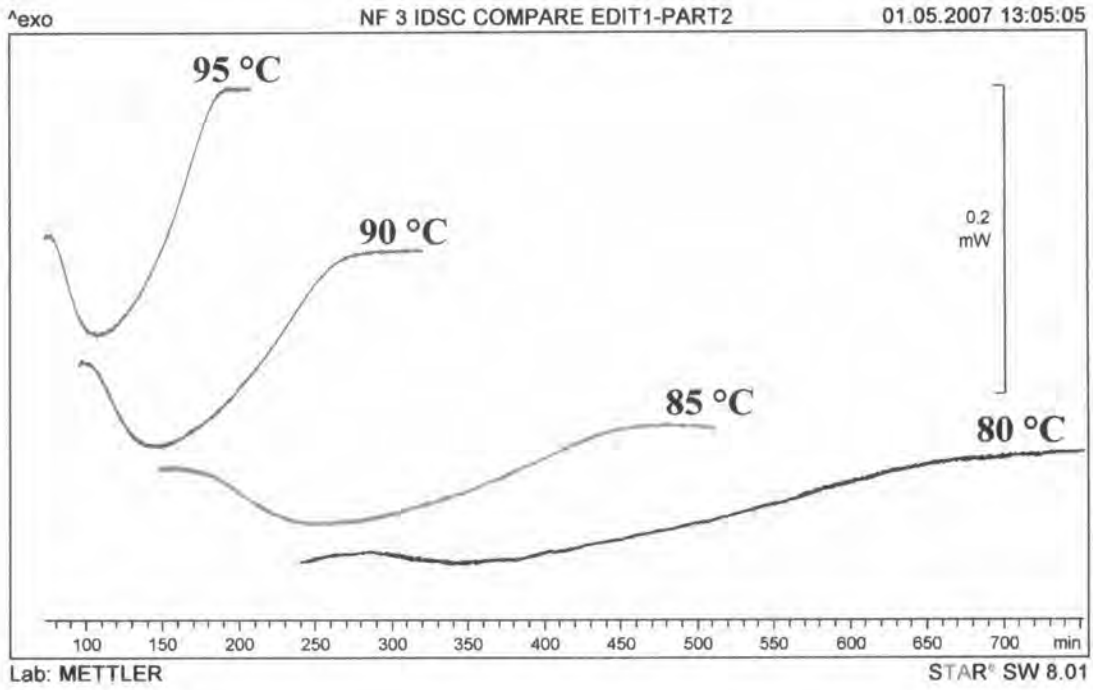

Figure 5.12 (cont.) IDSC of the second step of the thermograms obtained from trihydrate NF during isothermal dehydration at various T_{iso}

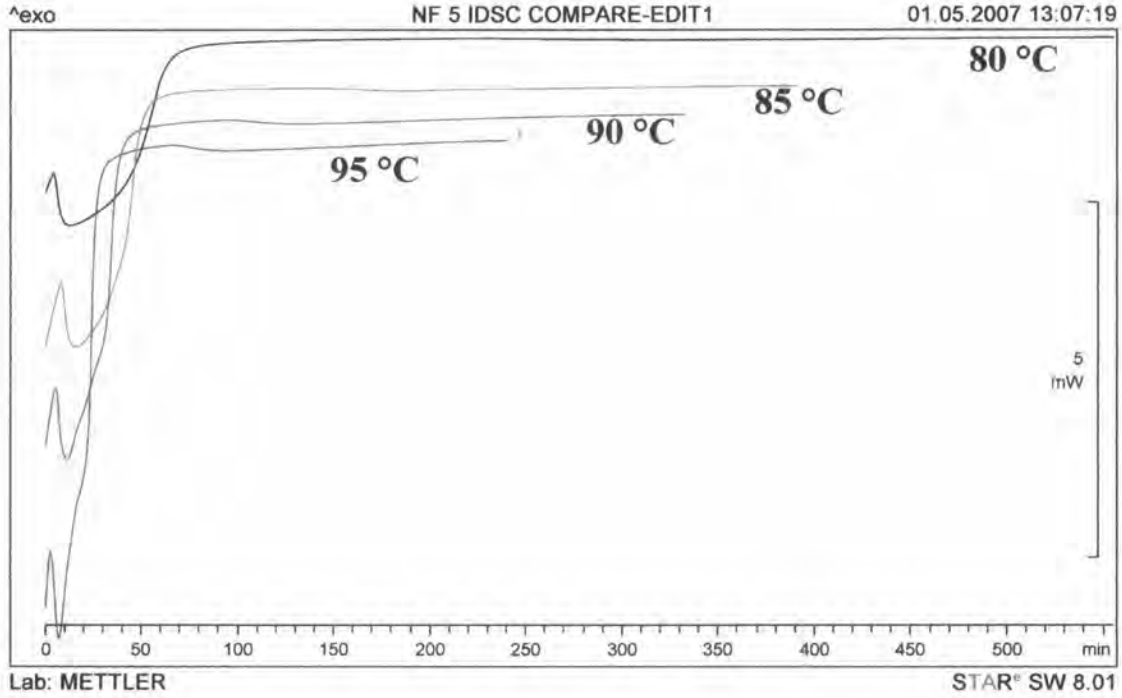

Figure 5.13 IDSC thermograms of pentahydrate NF during isothermal dehydration at various T_{iso}

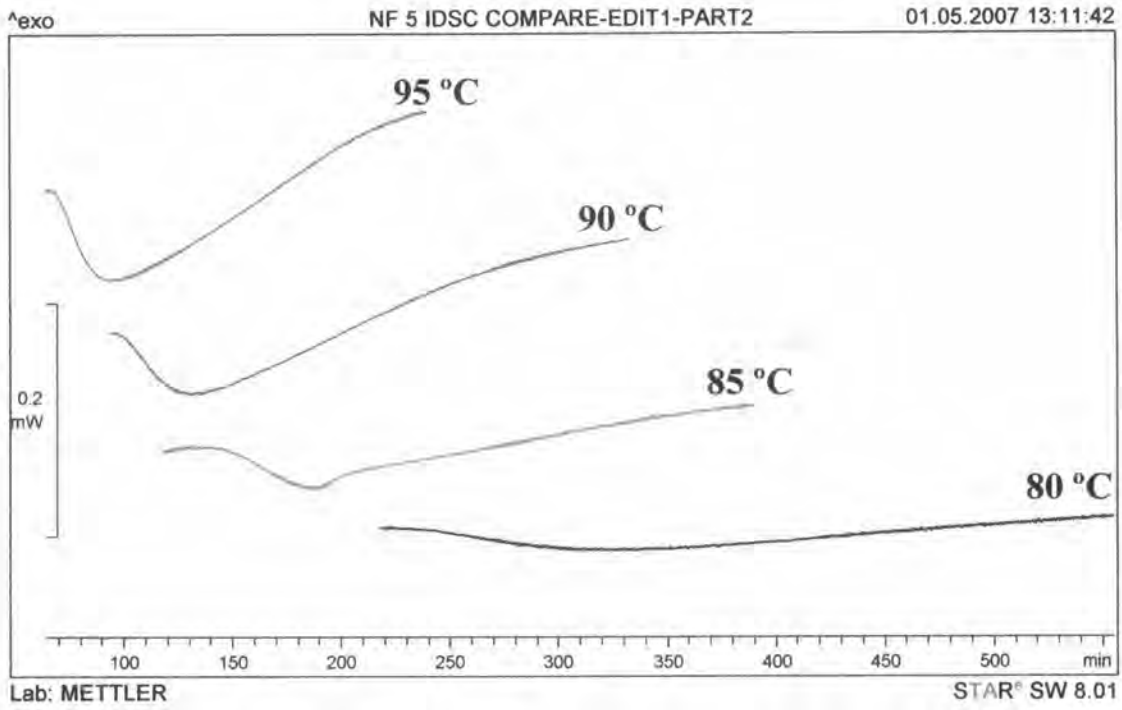

Figure 5.13 (cont.) IDSC of the second step of the thermograms obtained from pentahydrate NF during isothermal dehydration at various T_{iso}

Table 5.6 Dehydration energy, residual water content and particle size of dehydrated trihydrate NF after dehydration at different T_{iso}

Step of dehydration	T_{iso} (°C)	Dehydration energy (J/g)	Residual water content by TGA (% w/w)	d [v,0.5] (micron)
Intact form	-	-	14.88 ± 0.08	241.71 ± 1.95
First step	80	375.46 ± 17.78	3.03 ± 0.42	227.58 ± 4.66
	85	379.73 ± 10.21	2.64 ± 0.21	235.53 ± 2.97
	90	374.73 ± 2.34	2.91 ± 0.40	231.67 ± 2.27
	95	360.74 ± 4.16	3.43 ± 0.09	236.13 ± 1.39
Complete dehydration step	80	455.38 ± 7.56	0.56 ± 0.35	234.86 ± 2.17
	85	436.29 ± 42.09	0.36 ± 0.16	215.09 ± 3.89
	90	435.82 ± 18.74	0.11 ± 0.01	229.81 ± 0.35
	95	436.57 ± 3.87	0.15 ± 0.07	228.65 ± 2.13

Table 5.7 Dehydration energy, residual water content and particle size of dehydrated pentahydrate NF after dehydration at different T_{iso}

Step of dehydration	T_{iso} (°C)	Dehydration energy (J/g)	Residual water content by TGA (%w/w)	d [v,0.5] (micron)
Intact form	-	-	20.87 ± 0.15	211.04 ± 1.46
First step	80	409.32 ± 3.18	3.09 ± 0.08	199.52 ± 0.99
	85	392.63 ± 11.20	2.75 ± 0.17	198.91 ± 2.23
	90	387.12 ± 9.86	3.47 ± 0.19	168.52 ± 2.19
	95	400.25 ± 16.29	2.62 ± 0.15	203.14 ± 2.75
Complete dehydration step	80	416.59 ± 21.18	1.09 ± 1.16	205.58 ± 1.84
	85	436.90 ± 12.96	0.72 ± 0.30	187.77 ± 1.64
	90	434.50 ± 13.96	0.73 ± 0.12	197.51 ± 1.75
	95	448.12 ± 11.16	0.75 ± 0.01	192.52 ± 3.76

The direct energy measurement within each group of dehydration step with respect to temperatures used for T_{iso} for trihydrate NF and pentahydrate NF were insignificantly different. However, the differences of the energies between the first step dehydration and the complete step of dehydration for trihydrate NF and pentahydrate NF were statistically found ($p<0.05$). The results revealed that the total required energy for complete dehydration of both hydrates NF were not affected by the temperatures used similar to hemipentahydrate NF. The residual water contents of both trihydrate NF and pentahydrate NF after the first step of dehydration was approximately 2.5-3.5% w/w (Tables 5.6 and 5.7), indicating an incomplete dehydration of both hydrates after the first step of dehydration. Furthermore, XRPD patterns of both dehydrated trihydrate NF (Figure 5.14) and pentahydrate NF (Figure 5.15) after the first step of dehydration shown to be a mixture of anhydrous NF Form A and the hydrated transitional phase as described earlier in Chapter IV. However, only anhydrous NF Form A was found after allowing the complete dehydration for both NF hydrates (Figures 5.16 and 5.17). The low level of residual water contents of trihydrate NF and pentahydrate NF were at or below 1% w/w after the complete dehydration and confirmed the conversion to anhydrous NF Form A.

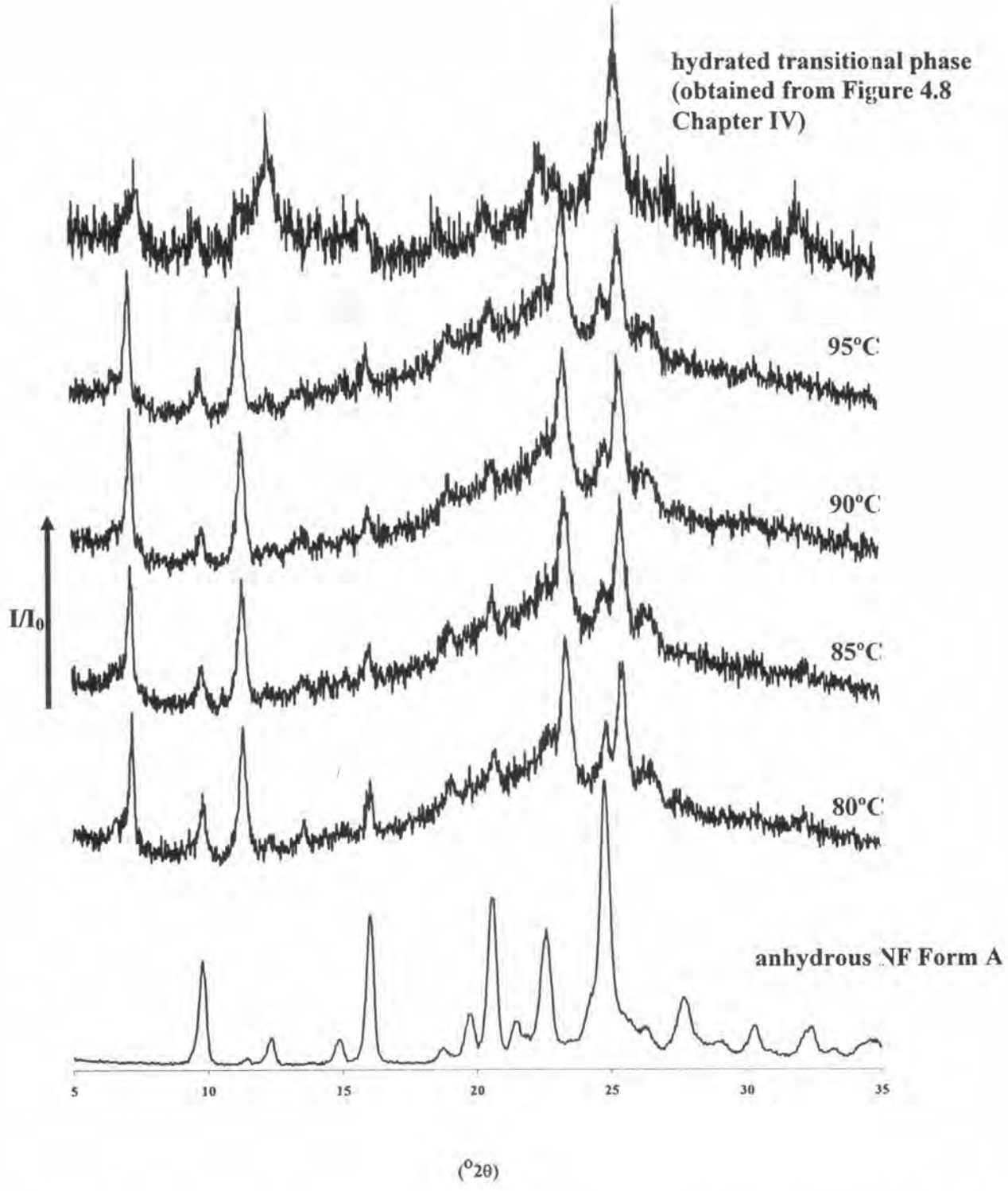

Figure 5.14 XRPD diffractograms of dehydrated trihydrate NF after first step of isothermal dehydration with respect to T_{iso}

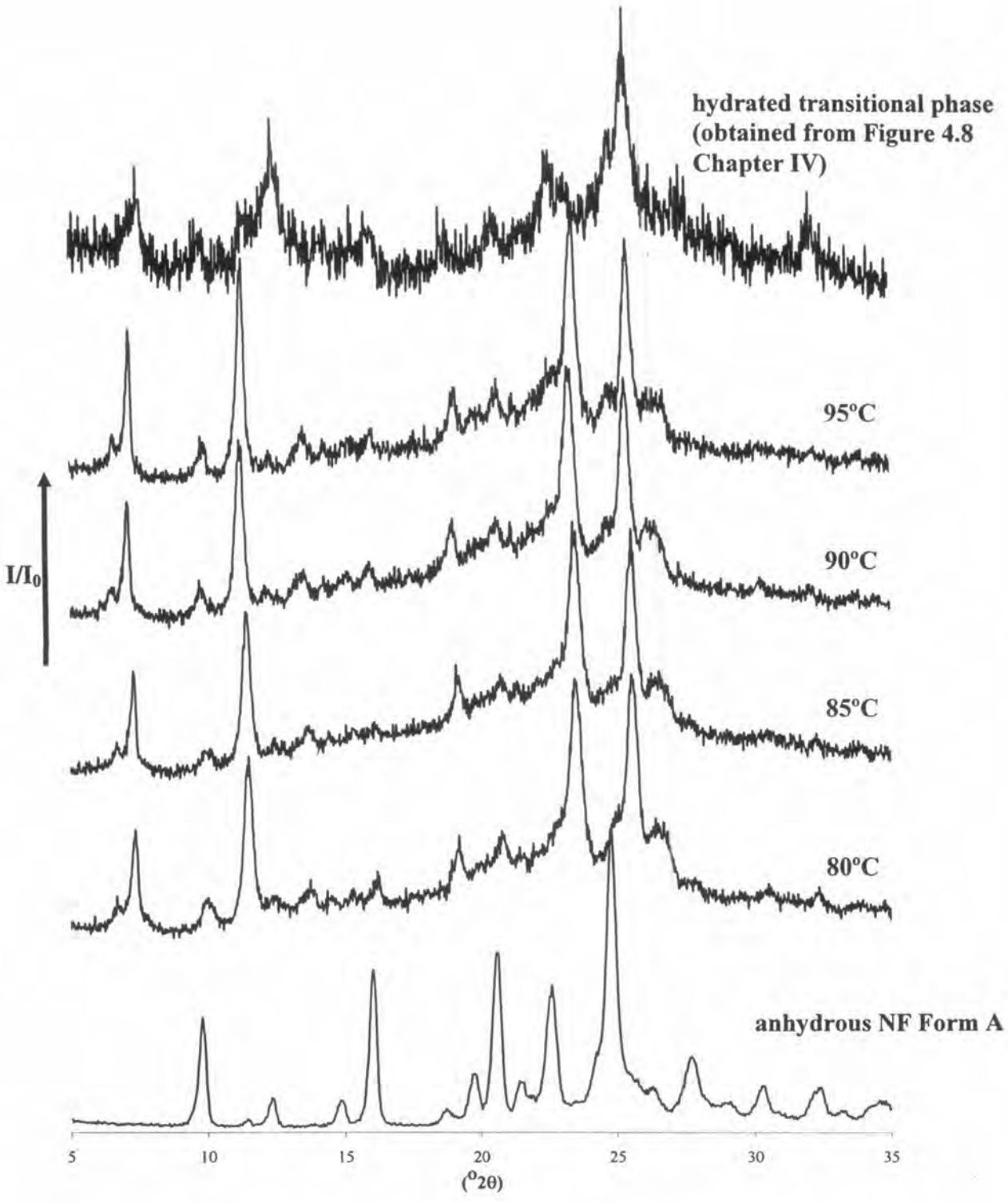

Figure 5.15 XRPD diffractograms of dehydrated pentahydrate NF after first step of isothermal dehydration with respect to T_{iso}

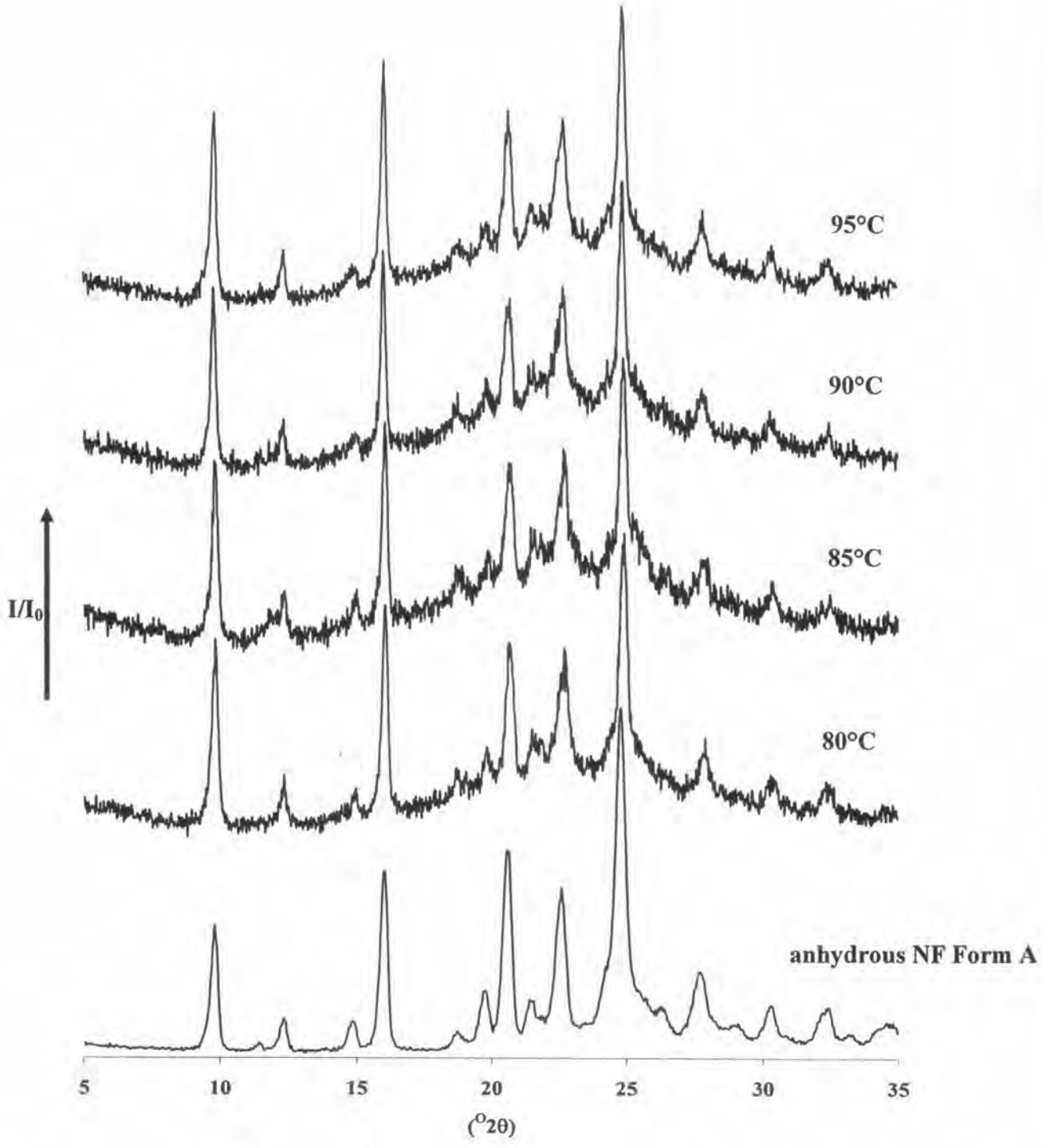

Figure 5.16 XRPD diffractograms of dehydrated trihydrate NF after complete dehydration with respect to T_{iso}

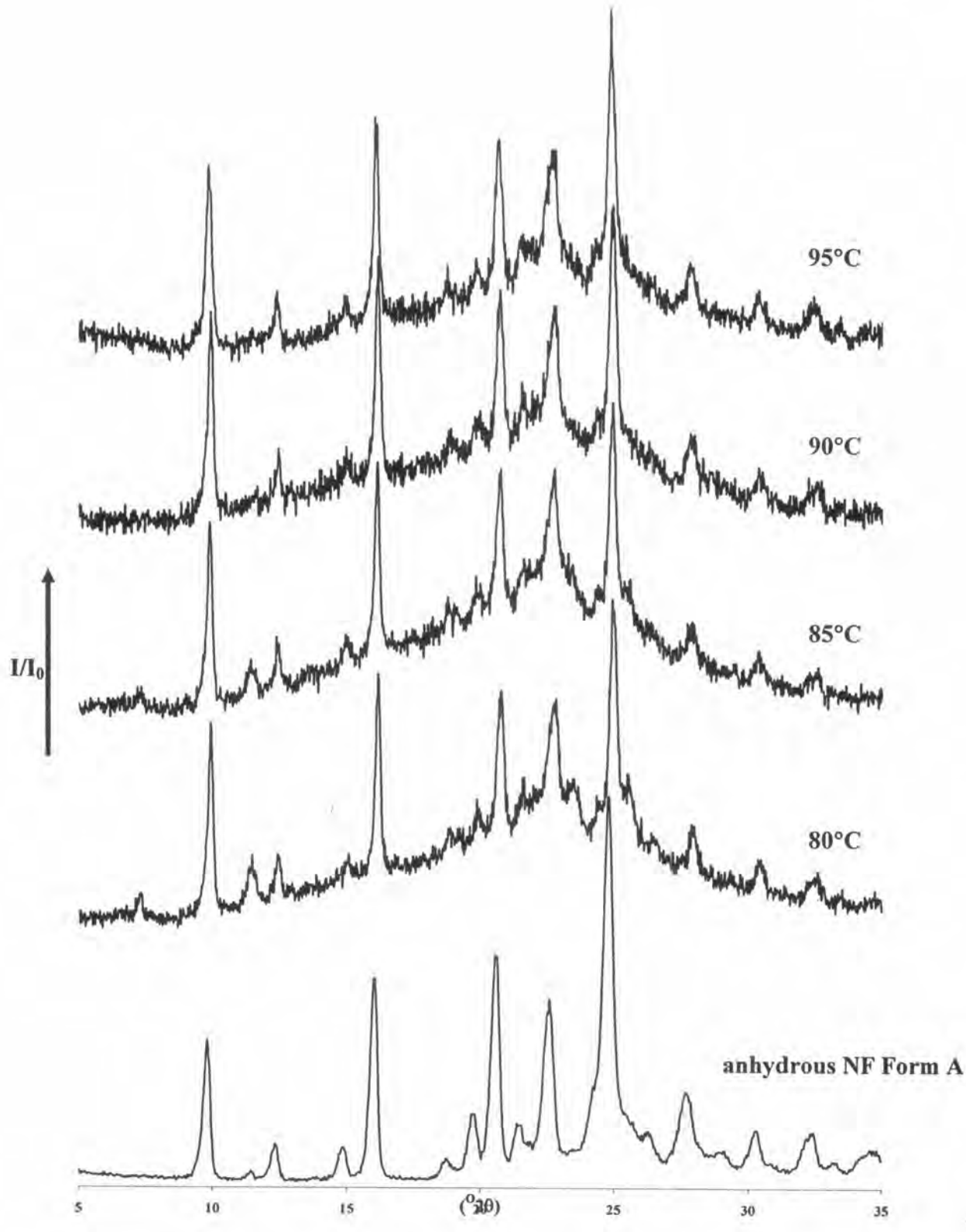

Figure 5.17 XRPD diffractograms of dehydrated trihydrate NF after complete dehydration with respect to T_{iso}

The particle size of dehydrated trihydrate NF and dehydrated pentahydrate NF were different from the particle size of intact form. However, these findings could not be concluded that particle size reduction of trihydrate NF and pentahydrate NF were clearly seen after dehydration. Because the maximum magnitude of particle size reduction of trihydrate NF and pentahydrate NF were approximately 25 microns and 40 microns, respectively. In summary, thermal dehydration could not reduce the particle size to a significant level for both trihydrate NF and pentahydrate NF.

Although thermal dehydration could not generate small particles of trihydrate NF and pentahydrate NF, the disruption of crystal took place as shown in SEM photomicrographs. Dehydration of trihyhydrates NF and pentahydrate NF with different steps of dehydration showed cracks on the surface of particles (Figures 5.18 -5.21) but it could not promote the individually scattered small particles as seen in BDM. However, the defects seen on large particles may potentially generate small particles with the manipulation of only very mild mechanical force. For example, mild pulverizing of deammoniated methabarbital gave the small particle than intact methabarbital (Sekiguchi et al., 1984).

The relationship between fraction reacted (α) and dehydration time (t) of trihydrate NF and pentahydrate NF are presented in Figures 5.22 and 5.23, respectively. In the case of trihydrate NF, the dehydration reaction may be separated in three steps due to unequal slopes whereas two different slopes were determined for the dehydration of pentahydrate NF. In term of model dependent kinetics, the E_a of each defined dehydration steps of trihydrate NF and pentahydrate NF are presented in Tables 5.8 and 5.9, respectively. Model dependent approach gave E_a of the dehydration of trihydrate NF of approximately 80 J/g, 98 J/g and 94 J/g for first, second and third step of dehydration, respectively. These results revealed that the "rate" of dehydration of all three steps were considered to be temperature dependent and the magnitude of dehydration rate dependent on temperature were similar. Meanwhile model independent approach showed the value of E_a of 85-115 kJ/mol which are similar to the energy barriers of each step of dehydration (Figure 5.10). The E_a from model independent of trihydrate NF showed initial decrease and gradually increased at later step of dehydration. It indicated the reduction of energy barrier due to the partially disrupted structure. However, the structure integrity was regenerated at the later stage seen from an increase of E_a. Thus, destroyed structure of trihydrate NF

during partial dehydration supported the particle size reduction even the stable structure later exists. For pentahydrate NF, model dependent showed E_a of dehydration at approximately 50 J/g, 70-90 J/g for early and later step of dehydration, respectively. These data were different from the data obtained with trihydrate NF. It indicated that the magnitude of temperature dependency in early step was lower than that of the later step of dehydration. Thus, the rate of dehydration of pentahydrate NF at early phase changed did not depend wholly on the dehydration temperature was raised equally. On the other hand, the E_a of pentahydrate NF from model independent, 50 kJ/mol, was equal to the E_a obtained from the early step of dehydration by model dependent. Moreover, the pattern of the change of E_a over the α of 0.1 to 0.8 was negligible changed. It should provide the stable structure and unchanged particle size of pentahydrate NF after dehydration. However, the particle size reduction of pentahydrate NF experimentally occurred. Hence, it should have another controlled factors of the particle size reduction of pentahydrate NF upon heating.

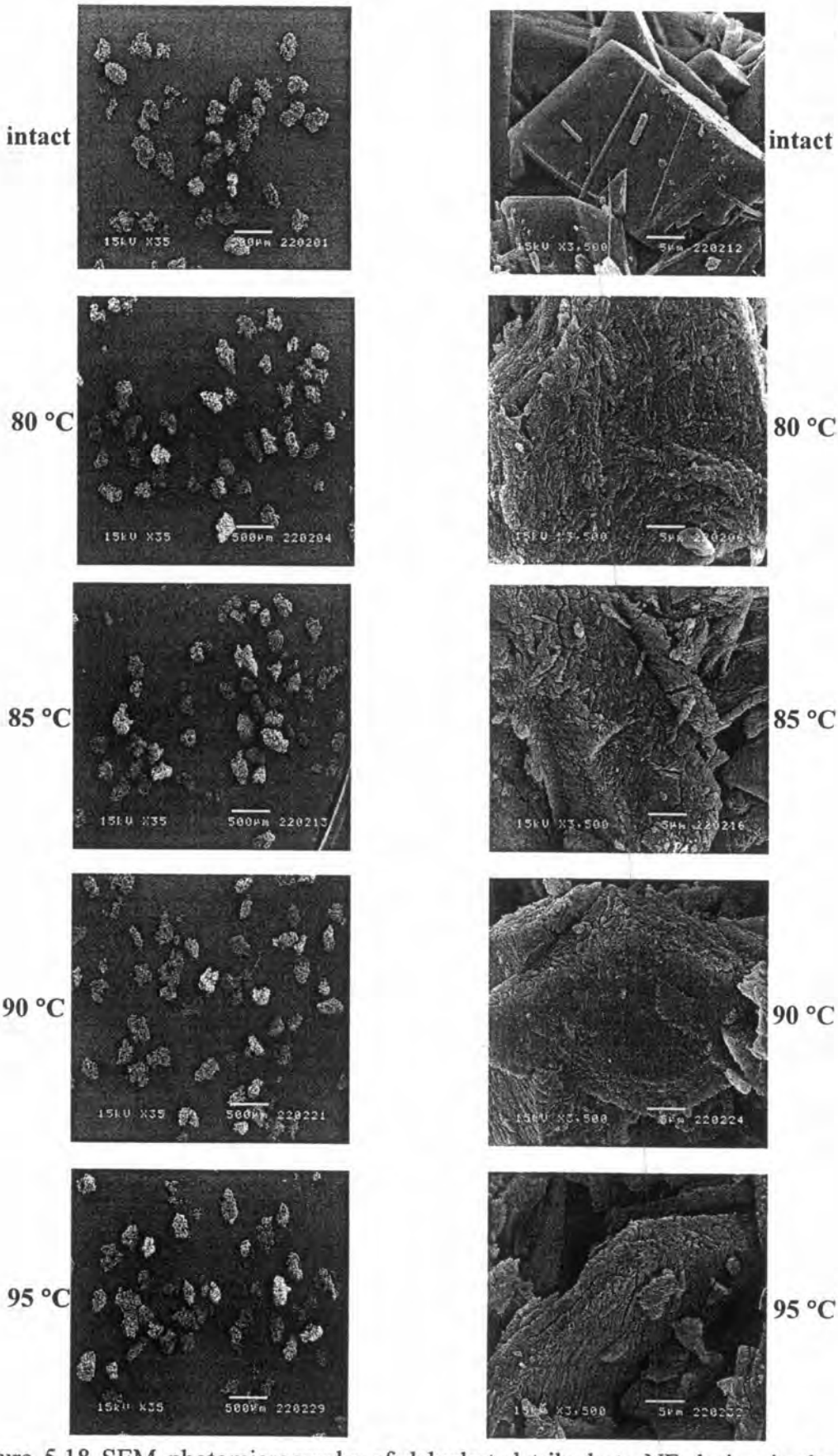

Figure 5.18 SEM photomicrographs of dehydrated trihydrate NF during isothermal dehydration after the first dehydration step with respect to T_{iso} (left column at the magnification of 35, right column at the magnification of 3500)

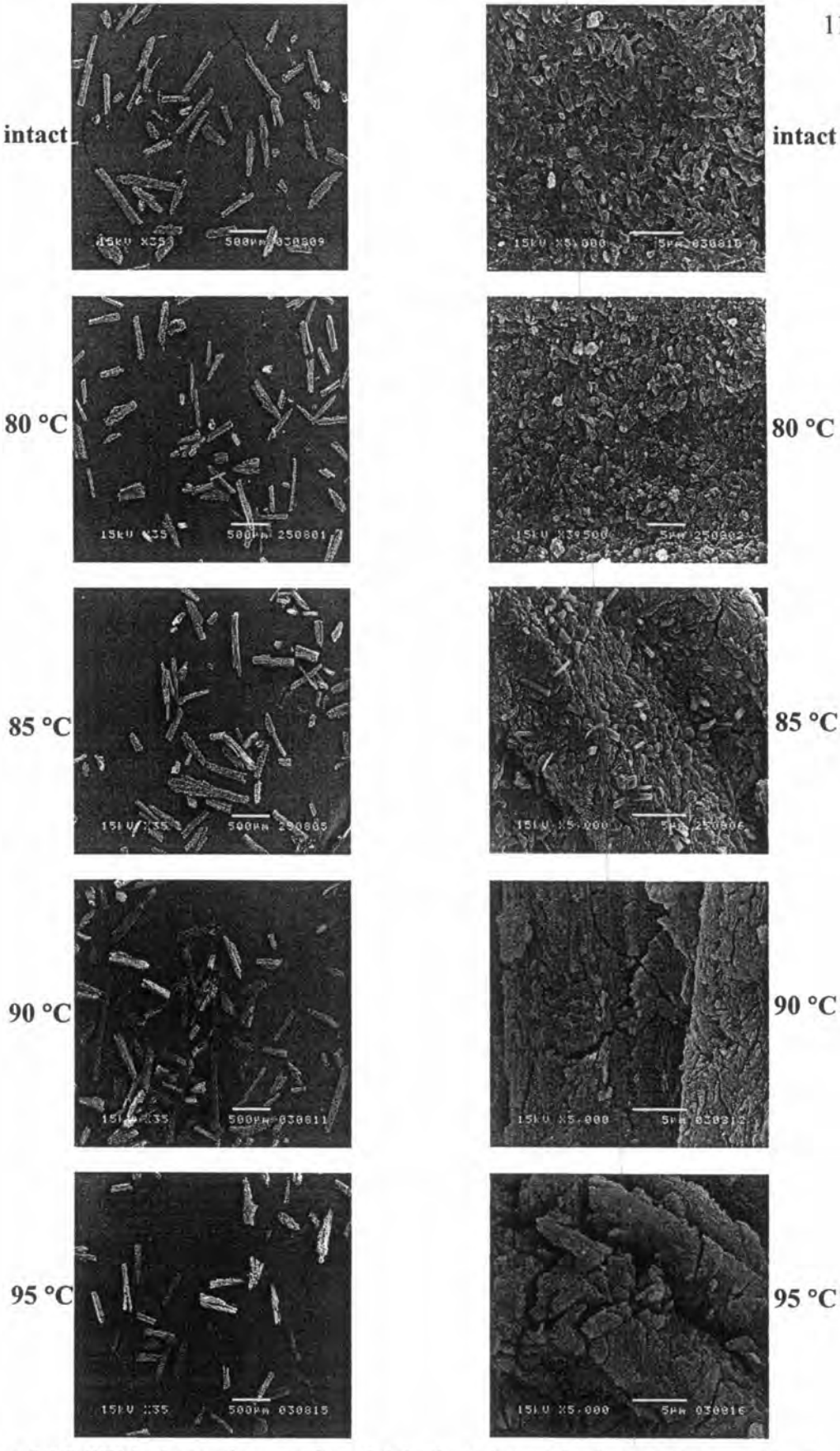

Figure 5.19 SEM photomicrographs of dehydrated pentahydrate NF during isothermal dehydration after the first dehydration step with respect to T_{iso}(left column at the magnification of 35, right column at the magnification of 5000 except of 80°C at 3500)

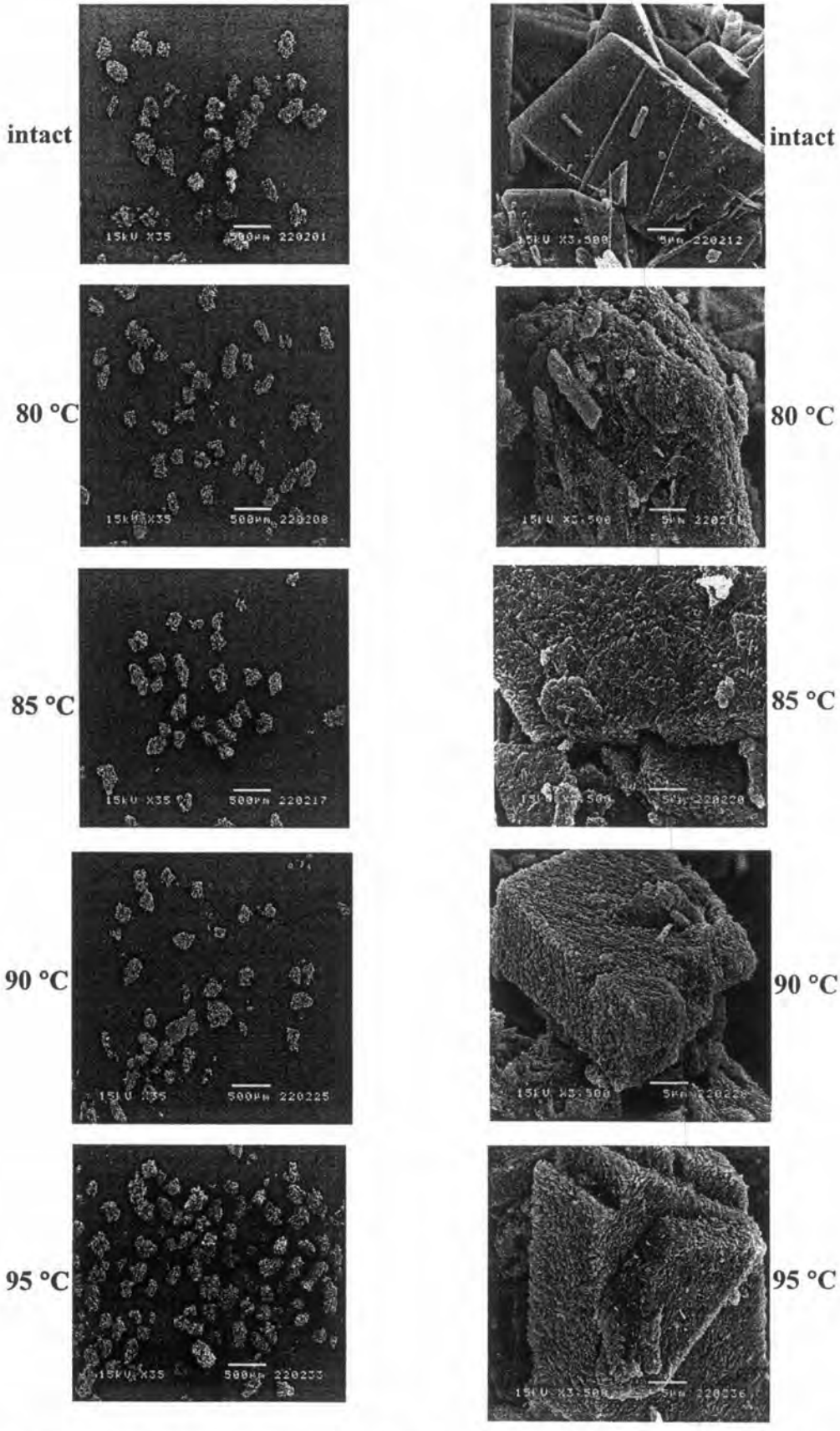

Figure 5.20 SEM photomicrographs of dehydrated trihydrate NF during isothermal dehydration after the complete dehydration with respect to T_{iso}(left column at the magnification of 35, right column at the magnification of 3500)

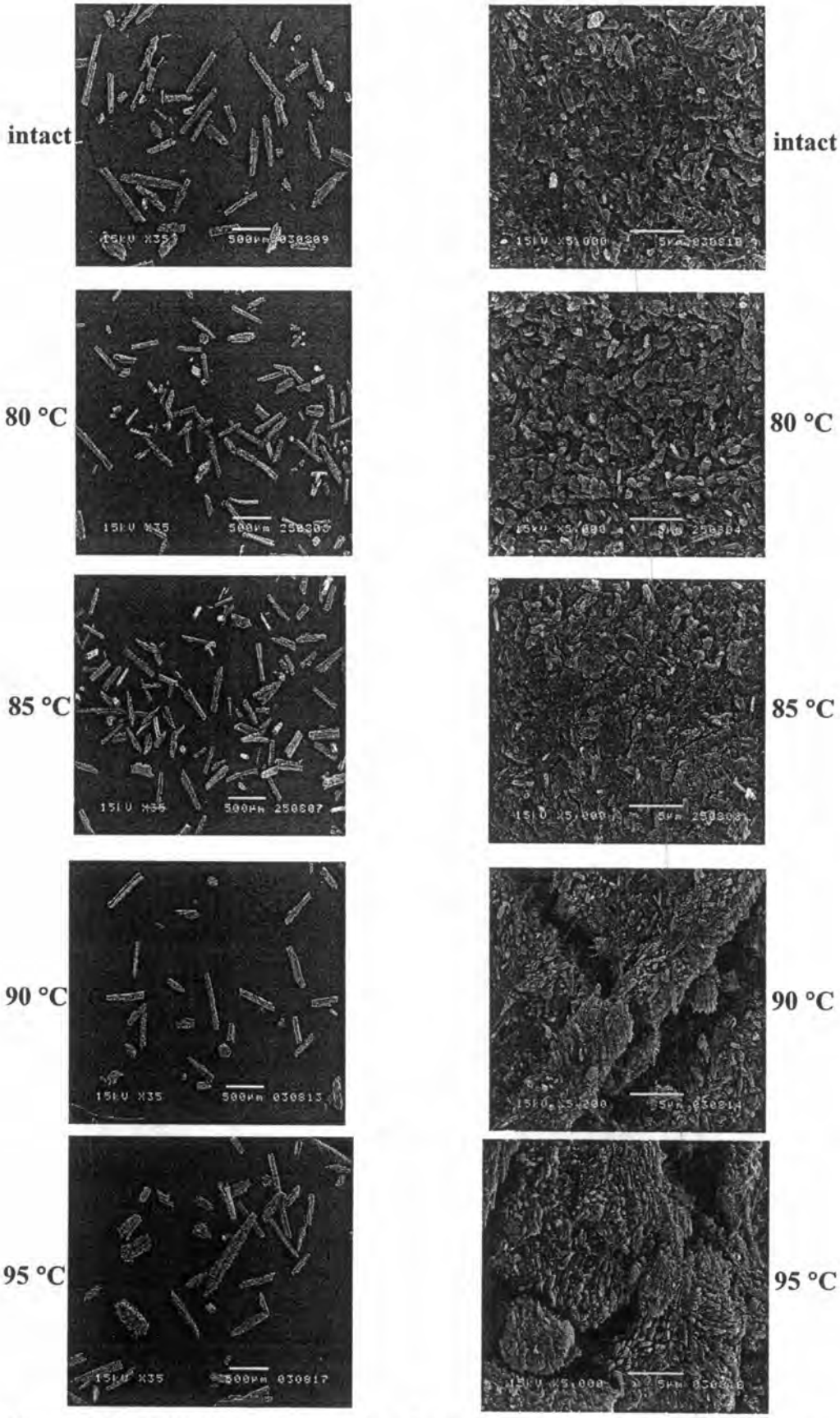

Figure 5.21 SEM photomicrographs of dehydrated pentahydrate NF during isothermal dehydration after the complete dehydration with respect to T_{iso} (left column at the magnification of 35, right column at the magnification of 5000)

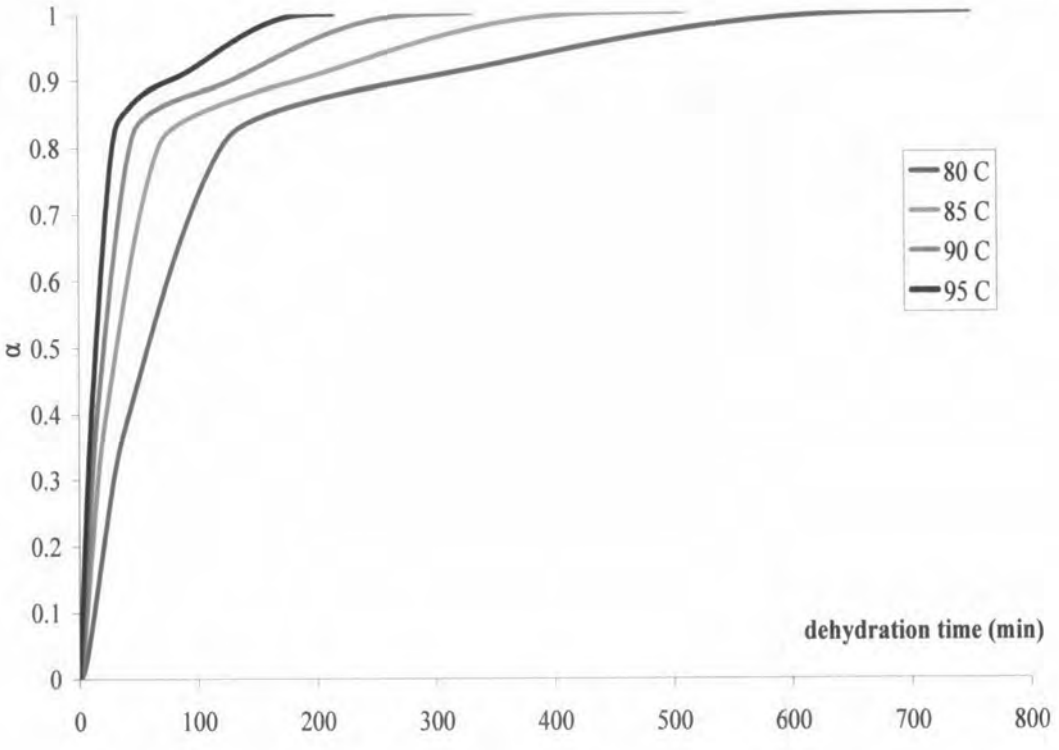

Figure 5.22 α-t curves during dehydration of trihydrate NF at different T_{iso}

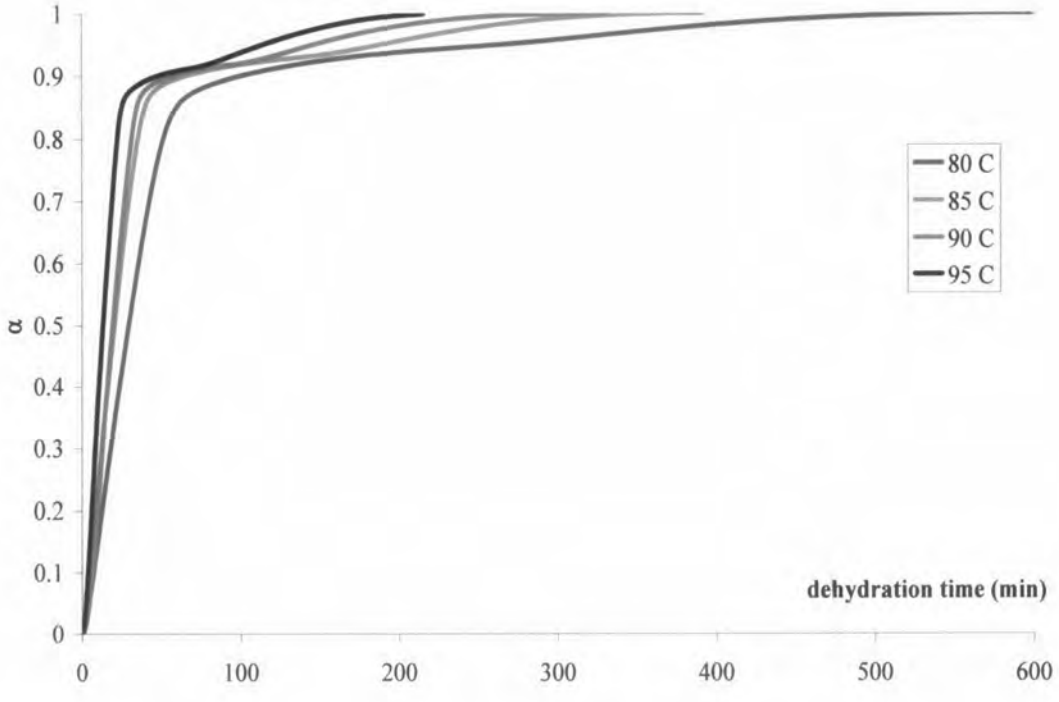

Figure 5.23 α-t curves during dehydration of pentahydrate NF at different T_{iso}

Table 5.8 The activation energy of isothermal dehydration of trihydrate NF with various solid state kinetic models

Model equation	E_a (kJ/mol)		
	First step of dehydration (0.10 to 0.30 of α)	Second step of dehydration (0.40 to 0.70 of α)	Third step of dehydration (0.93 to 0.97 of α)
Avrami Erofëev			
1 dimensional	80.52	97.02	93.69
2 dimensional	79.74	97.66	93.75
Order reaction			
1st order	82.79	101.28	93.45
Phase Boundary			
1 dimensional	81.77	97.71	94.80

Table 5.9 The activation energy of isothermal dehydration of pentahydrate NF with various solid state kinetic models

Model equation	E_a (kJ/mol)	
	First step of dehydration (0.20 to 0.80 of α)	Second step of dehydration (0.93 to 0.97 of α)*
Diffusion Controlled		
1 dimensional	51.21	87.52
Phase Boundary		
1 dimensional	51.18	88.66
2 dimensional	51.38	71.68

* The values are calculated from the IDSC data of T_{iso} 85, 90 and 95 °C

The crystallographic data of materials are generally solved by SC-XRD and used as platform to evaluate and confirm the possibility of size reduction during thermal dehydration similar to the dehydration of BDM in Chapter 3. In this study, hemipentahydrate NF, trihydrate NF and pentahydrate NF were generated with an inappropriate property to be tested by SC-XRD even several attempts were performed. To alternatively gain crystallographic data, XRPD was employed with the aid of specific software, PowderSolve®. Unfortunately, XRPD of all NF hydrates

could not be indexed and did not provide valid lattice parameter. Therefore, it was not possible to determine the NF hydrate structures. The lattice structures which will lead to the explanation of the possibility of particle size reduction via thermal dehydration of hemipentahydrate NF, trihydrate NF and pentahydrate NF was impossible.

According to an ineffective process of particle size reduction by thermal dehydration of the stoichiometric NF hydrates, the relationship between the apparent particle size reduction energy and stoichiometry could not be established. However, dehydration energy of different stochiometric NF hydrates would be considered instead of the apparent energy for particle size reduction. The calculated total dehydration energy from IDSC of various NF hydrates (Tables 5.4, 5.6 and 5.7) were found to be lower than the enthalpy of dehydration obtained by regular non-isothermal DSC (NIDSC) in Figure 5.24. It may be due to the condition of IDSC that generated temperature shift (from ambient temperature to the desired dehydration temperature) before the signal of IDSC was recorded. The energy loss during the initial temperature adjustment of NF hydrate samples by IDSC were determined as a function of dehydration temperature in conjunction with NIDSC at a heating rate of 10 °C/min prior to IDSC measurements (Figure 5.25). The initial energy calculation during initial NIDSC portion was obtained from the AUC starting at point X to point A as seen in Figure 5.25. The initial energy loss during heating of hemipentahydrate NF was 96.75, 101.70, 120.11 and 137.56 J/g at 80, 85, 90 and 95 °C, respectively. When the initial energy loss were added to the dehydration energy calculated from IDSC at each dehydration temperature, the total energy were in the range of 380-415 J/g and found to be close to the enthalpy of dehydration of hemipentahydrate NF obtained by regular NIDSC which was 408.79 J/g (Figure 5.24). For trihydrate NF, the initial energy loss were 87.01, 107.11, 120.16 and 133.25 at 80, 85, 90 and 95 °C, respectively while they were 101.66, 118.53, 137.93 and 151.60 at 80, 85, 90 and 95 °C, respectively for pentahydrate NF. The sum between the initial energy loss and calculated total dehydration energy from IDSC were 540-570 and 520-600 J/g for trihydrate NF and pentahydrate NF. These results were similar to the total enthalpy of dehydration from regular NIDSC of trihydrate NF (557.95 J/g) and pentahydrate NF (614.65 J/g). Thus, it should be reminded that IDSC method for the determination of dehydration energy of NF hydrates would lack the initial portion of the total

dehydration energy. However, the dehydration energy from IDSC could preliminary be used to roughly evaluate the relationship between the stoichiometry of hydrates and required energy for dehydration.

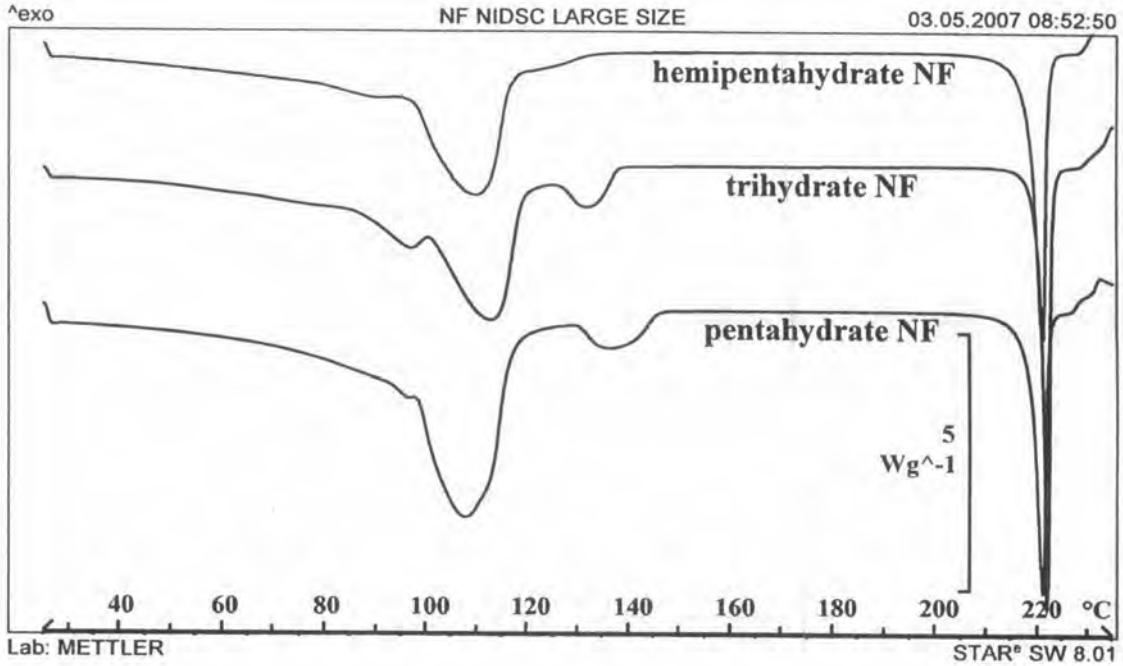

Figure 5.24 The regular non isothermal DSC (NIDSC) thermograms of some NF hydrates at the heating rate of 10 °C /min

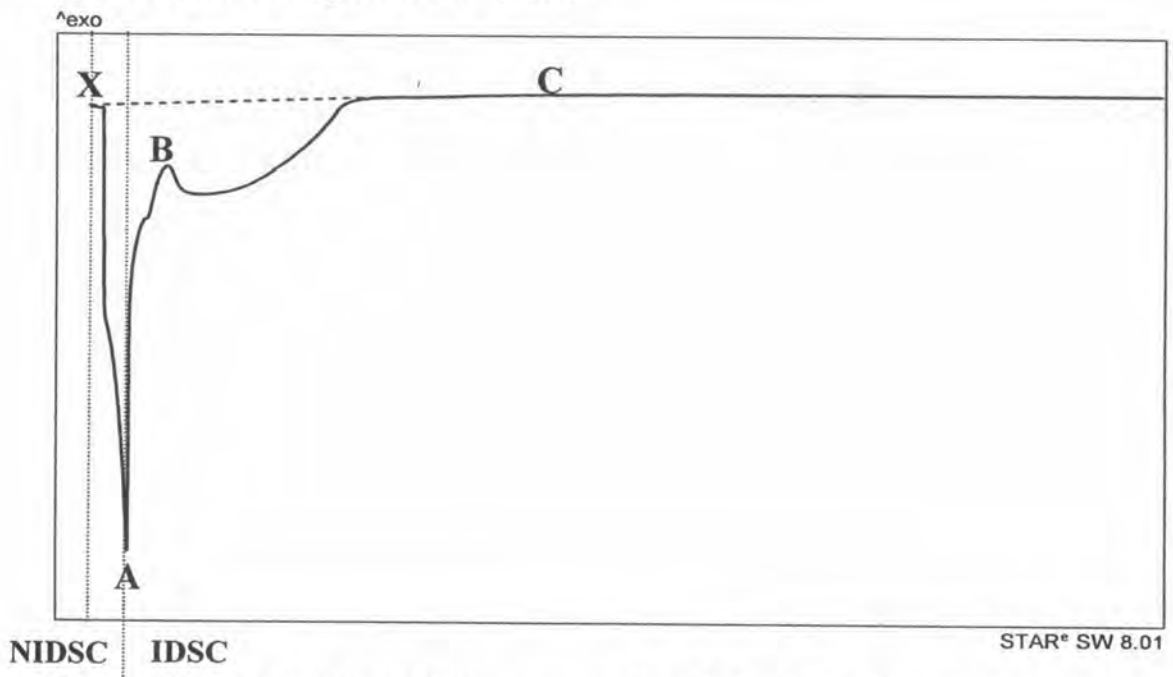

Figure 5.25 Model of NIDSC thermogram (X to A) before IDSC thermorgram (A to C) of NF hydrate during isothermal dehydration

The relationship between the stoichiometry of NF hydrates and total dehydration energy used from IDSC is presented in Figure 5.26. Hemipentahydrate NF showed the lowest dehydration energy that followed the theoretical basis of chemical dehydration. Dehydration energy should be lower for the lower stoichiomtry of the same hydrate compound. It is due to a less number of binding forces (particularly hydrogen bonds) between water molecules and the active moiety in the hydrated structure. However, dehydration energy of trihydrate NF was found not to be different than the pentahydrate NF. This result did not obey the general basis of dehydration as described above. This may be due to the lost of initial dehydration energy which was not accounted for by IDSC as discussed earlier. If the total energy, obtained by the regular NIDSC experiments were plotted against stoichiometry of NF hydrates, the relationship was found to be correlated to the energy and stoichiometry assumption of linearity more than when IDSC was used alone (Figure 5.26(open circle). However, through this evaluation, the total dehydration energy of the pentahydrate NF was not critically higher than that of the trihydrate NF as was assumed if linearity was achieved. Another aspect to consider for dehydration of hydrates was regarding the types of hydrogen bonding in the hydrated structure. The shorter hydrogen bonds theoretically give stronger binding force and need more energy to break down (Jeffrey, 1997). This concept may explain the similarity of dehydration energy between lower stoichiometric trihydrate NF to the higher stoichiometric pentahydrate NF. However, this is only an assumption of this issue due to the crystallographic data of NF hydrates were not possible to be elucidated at this time.

Another factor which may govern the accurate calculation of the total dehydration energy is the positioning of water molecules within the crystal lattice. The model NF hydrates used in this study may have several sites for water molecules to reside. Thus, dehydration occurred in several steps and may lead to inaccurate calculation of energy for dehydration. A future good model proposed for the methods used in this experiment to prove the correlation of dehydration energy to the stoichiometry should have only one lattice site for water molecules to reside no matter what the stoichiometry should be.

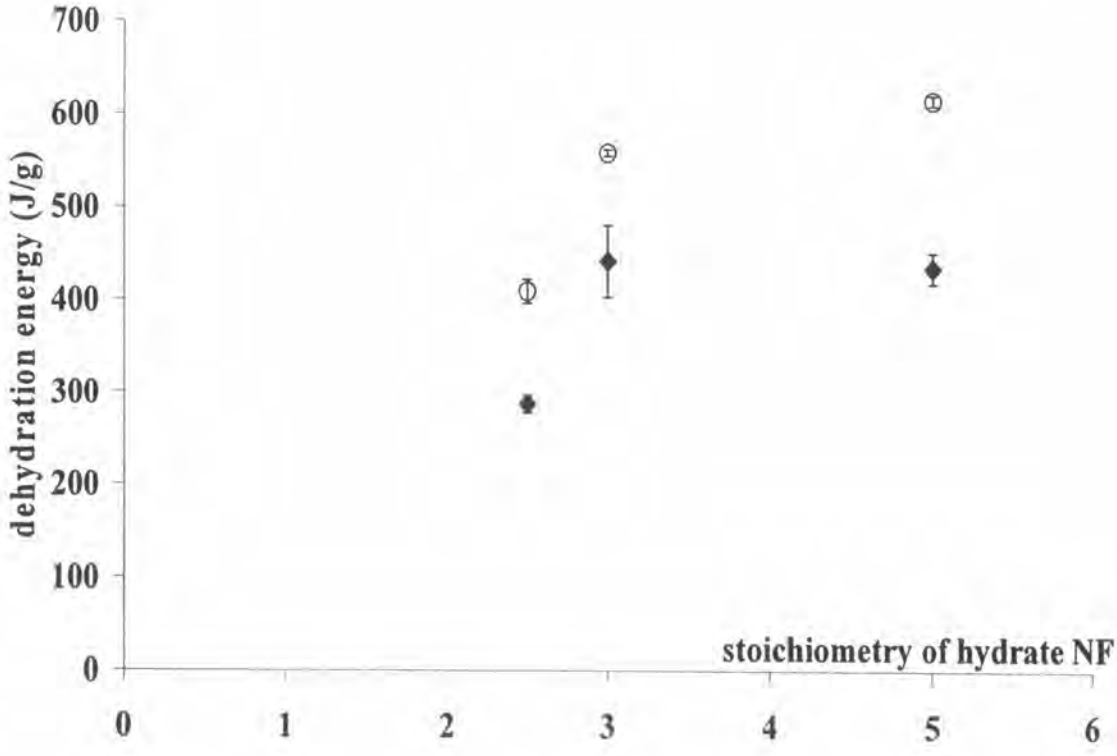

Figure 5.26 The relationship between stoichiometry and dehydration energy of NF hydrates obtained by different calculation methods (◆ IDSC method alone, O regular NIDSC)

5.4 CONCLUSIONS

The dehydration behaviors of hemipentahydrate NF, trihydrate NF and pentahydrate NF comprised of several steps of dehydration. Unclear step of dehydration was found in the dehydration of hemipentahydrate NF. Meanwhile, two steps of dehydration of trihydrate NF and pentahydrate NF were clearly separated. An incomplete dehydration of hemipentahydrate NF, trihydrate NF and pentahydrate NF generated the mixture of hydrated transitional phase (which was assumed to be hemihydrate NF) and the anhydrous NF form A. However, where dehydration of the above three NF hydrates were completed, it induced pure anhydrous NF Form A.

Thermal dehydration was shown to be an ineffective method for particle size reduction of NF hydrates, despite its effectiveness in BDM. The difference of approximately 25, 25 and 40 microns in particle size was found for dehydrated hemipentahydrate NF, dehydrated trihydrate NF and dehydrated pentahydrate NF, compared to the initial hydrated particles. Although it was found to be statistically significant, it was not sufficiently clear to indicate the effectiveness in particle size reduction by thermal dehydration. As a result, thermal dehydration of NF hydrates could only disrupt the surface of the crystal without generating individually smaller particles. The dehydrated particles may be further treated to reduce the particle size with mild mechanical grinding. Thus, the apparent particle size reduction energy was not possible to be evaluated.

The calculated E_a of all NF hydrates from solid state kinetic approaches were positive values which signified temperature dependency of the "dehydration rate" of every NF hydrates. However, the calculated E_a values obtained for each stoichiomteric NF hydrate were similar despite the difference in temperature levels. This result indicated that the amount of energy required for dehydration reaction to occur for each stoichiometric NF hydrate is the same. After total dehydration energy was obtained it was found that the total required energy for lower stoichiometry (hemipentahydrate NF) was lower than that of higher stoichiometry (trihydrate NF and pentahydrate NF). Theoretically, total dehydration energy of hydrates should depend on the number of binding forces, particularly hydrogen bonding. Thus, the lower stoichiometry should require lower energy to induce dehydration. However, dehydration energy of trihydrate NF was similar to the higher stoichiometric

pentahydrate NF. This may be due to the location of water molecules dispersed within the crystal lattice, the number of hydrogen bonding between water and active moiety and the strength of hydrogen bonding which played an important role on total dehydration energy.

The total dehydration energy of NF hydrates was found to be much higher than the energy needed for BDM despite the calculation methods used. This could be inclined that the bonding energy between water and NF molecules were stronger, bond distance were shorter and the structures were densely packed with less void volume (as can be compared to the coefficient of packing (K_{chan}) values of BDM and dihydrate NF). The NF hydrate structures of being very close in proximity were physically very stable and less likely to collapse after water removal. Unlike BDM, NF hydrates did not show obvious particle size reduction or structural collapse upon thermal dehydration due to reasons state above.

In conclusion, the degree of dehydration energy and the crystal structure void volume after dehydration are two of the factors which may be used and compared to the reference materials (such as risedronate sodium hemipentahydrate and BDM) to preliminary determine the possibility of particle size reduction of hydrated structures of organic compounds.